WITNESSES OF THE NEO-TETHYS OCEAN IN SOUTHEAST IRAN: A REVIEW OF THE LATE JURASSIC-CRETACEOUS OPHIOLITES OF THE NORTH MAKRAN DOMAIN

Edoardo Barbero*, Luca Pandolfi, Morteza Delavari***, Asghar Dolati***, Emilio Saccani°,✉, Maria Di Rosa**** and **Michele Marroni****

* *Istituto di Geoscienze e Georisorse, CNR, Torino, Italy.*
** *Dipartimento di Scienze della Terra, Università di Pisa, Italy.*
*** *Faculty of Earth Sciences, Kharazmi University, Tehran, Iran.*
° *Dipartimento di Fisica e Scienze della Terra, Università di Ferrara, Italy.*
✉ *Corresponding author, e-mail: emilio.saccani@unife.it*

Keywords: *Tectonics; stratigraphy; geochemistry; Neo-Tethys geodynamics; North Makran Domain, Iran.*

ABSTRACT

This review compiles and integrates available stratigraphic, structural, petrological, geochemical, and geochronological data on subduction-related and subduction-unrelated ophiolites in the North Makran domain (southeastern Iran) to reconstruct the formation, evolution, and incorporation of Neo-Tethyan oceanic lithosphere within the Makran Accretionary Prism. The data indicate a multi-stage geodynamic evolution, beginning in the Late Jurassic-Early Cretaceous, when oceanic lithosphere formed predominantly in a mid-ocean ridge setting, locally influenced by plume-related components. During the Early Cretaceous, the initiation of an intra-oceanic subduction zone led to the formation of forearc lithosphere and to the progressive separation of the North Makran Ocean from the main Neo-Tethys. In the Late Cretaceous, oceanic lithosphere formation became more complex, with the coeval development of plume-related magmatism in seamounts and volcanic arc activity associated with subduction of the North Makran Ocean beneath the Lut Block. This stage records the coexistence of subduction-unrelated and subduction-related magmatic systems within the same oceanic basin. Final closure of the composite oceanic lithosphere of the North Makran Ocean took place from the latest Cretaceous to the Paleocene, through progressive subduction, accretion, and underplating within the Makran Accretionary Prism. Overall, the North Makran domain provides a unique natural laboratory for investigating how ridge, plume, and multiple subduction processes interact through time to generate oceanic lithosphere within a convergent plate margin, highlighting the complexity of Neo-Tethyan geodynamic evolution.

INTRODUCTION

Ophiolites are key tectonic components of both accretionary- and collisional-type orogenic belts, representing relicts of ancient oceanic lithosphere that evolved between continental plates and terranes (e.g., Dilek and Furnes, 2011 and references therein; Barbero et al., 2023a). As such, they provide fundamental archives of plate tectonic processes, recording the evolution of oceanic lithosphere from continental extension and mantle exhumation to seafloor spreading, subduction, and continental collision (e.g., Dilek, 2003).

According to the integrated classification of ophiolites proposed by Dilek and Furnes (2011, 2014), ophiolites can be subdivided in subduction-unrelated and subduction-related types (see also Pearce, 2008). These two groups display distinct stratigraphic-structural architectures, lithological makeups, and geochemical characteristics, reflecting differences in the mode and tempo of the magmatic and tectonic processes operating during oceanic lithosphere formation and evolution (e.g., Shervais, 2001; Marroni and Pandolfi, 2007; Dilek and Furnes, 2011; Balestro et al., 2015; Safonova et al., 2016; Saccani et al., 2017).

Subduction-unrelated ophiolites comprise oceanic lithosphere whose magmatic evolution were not influenced by subduction processes (Dilek and Furnes, 2011, 2014; Saccani, 2015). These types include ophiolites formed at continental margin, mid-ocean ridge, mature back-arc basin, and oceanic within-plate (plume-type ophiolites) settings.

In contrast, subduction-related ophiolites are genetically related to magmatic and tectonic processes acting in the upper plate of a subduction zone (Dilek and Furnes, 2011, 2014). They include supra-subduction zone ophiolites (including forearc and back-arc ophiolites) and volcanic arc ophiolites (e.g., Dilek and Furnes, 2011; Saccani et al., 2017; Furnes et al., 2020).

The distinction between subduction-unrelated and subduction-related ophiolites thus represents a fundamental guideline for reconstructing the paleogeography and tectono-magmatic evolution of ancient oceanic basins and their margins, as well as for the geodynamic evolution of accretionary- and collisional-type orogenic belts. To this end, multidisciplinary approaches integrating stratigraphic and structural data, geochronology, and geochemical and petrological studies are essential.

Among the most significant ophiolite occurrences worldwide are those preserved within the Alpine-Himalayan orogenic belts, which are interpreted as relicts of the Neo-Tethys Ocean. This long-lived and complex oceanic basin developed from the Late Permian - Triassic between the Africa-Arabia Plates and Eurasia (Stöcklin, 1968; Dercourt et al., 1986; Şengör et al., 1988; Ricou, 1994; Stampfli, 2000; Metcalfe, 2013; Barrier et al., 2018). In the Middle East, the Neo-Tethyan ophiolites are distributed along a ~7,000 km-long orogenic belt extending from the Anatolian suture zones to the Zagros collisional belt, the Makran Accretionary Prism, and the Pakistani sector of Himalaya (e.g., Agard et al., 2011; Saccani et al., 2013; Kakar et al., 2014; Moghadam and Stern, 2015; Burg, 2018; Parlak et al., 2019; Bonnet et al., 2020a, b; Rolland et al., 2020; Moghadam et al., 2021; Salam et al., 2024; Barbero et al., 2025). These ophiolites range in age from Jurassic to Cretaceous and include both subduction-unrelated (e.g., Ghazi et al., 2004; Saccani et al., 2010, 2013;

Barbero et al., 2020b, 2021a, 2021b, 2023b, 2023c) and subduction-related types (e.g., Moghadam et al., 2013; Kakar et al., 2014; Delavari et al., 2016; Monsef et al., 2018; Pirnia et al 2019; Barbero et al., 2020a; Ghasemi Siani et al., 2025), indicating a long-lived and multi-stage evolution of the Neo-Tethys Ocean in the Middle East.

Within this regional framework, the Makran sector represents a key area for investigating the late stages of Neo-Tethyan evolution. It is characterized by a ~1,000 km-long accretionary prism, namely the Makran Accretionary Prism (Fig. 1), formed by Cretaceous to present-day convergence between the Arabian Plate and the southern margin of the Lut Block (e.g., McCall and Kidd, 1982; Glennie et al., 1990; Ricou, 1994; Kopp et al., 2000). This prism is associated with the still active northward subduction of the Neo-Tethys oceanic lithosphere (Kopp et al., 2000; Grando and McClay, 2007; Burg, 2018). In the Makran Accretionary Prism, Neo-Tethyan ophiolites are widely exposed in tectonic units forming the backstop of the prism, which corresponds to the North Makran domain (Fig. 2; Burg, 2018; Barbero et al., 2025). These ophiolites include different varieties of both subduction-related and subduction-unrelated types. Therefore, they provide a key natural laboratory for investigating the evolution of the Neo-Tethys in the only sector of the Alpine-Himalayan orogenic belt where oceanic subduction is still active.

In this study, we present a comprehensive review of the ophiolites of the western North Makran domain, based on an extensive compilation of published structural, stratigraphic, petrographic, geochemical, and geochronological data. On this basis, we propose a revised reconstruction of the geodynamic evolution of North Makran domain and discuss its implications for the evolution of the Middle East Neo-Tethys Ocean.

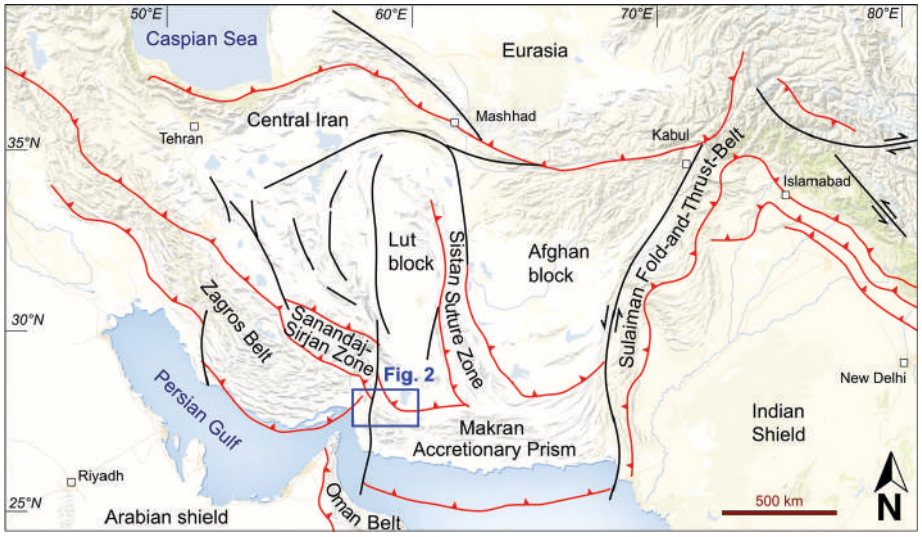

Fig. 1 - General tectonic map of the Middle East and western Himalayan region, showing the main deformation fronts. The main plates interacting in this area are indicated. The location of Fig. 2 is shown in the blue box.

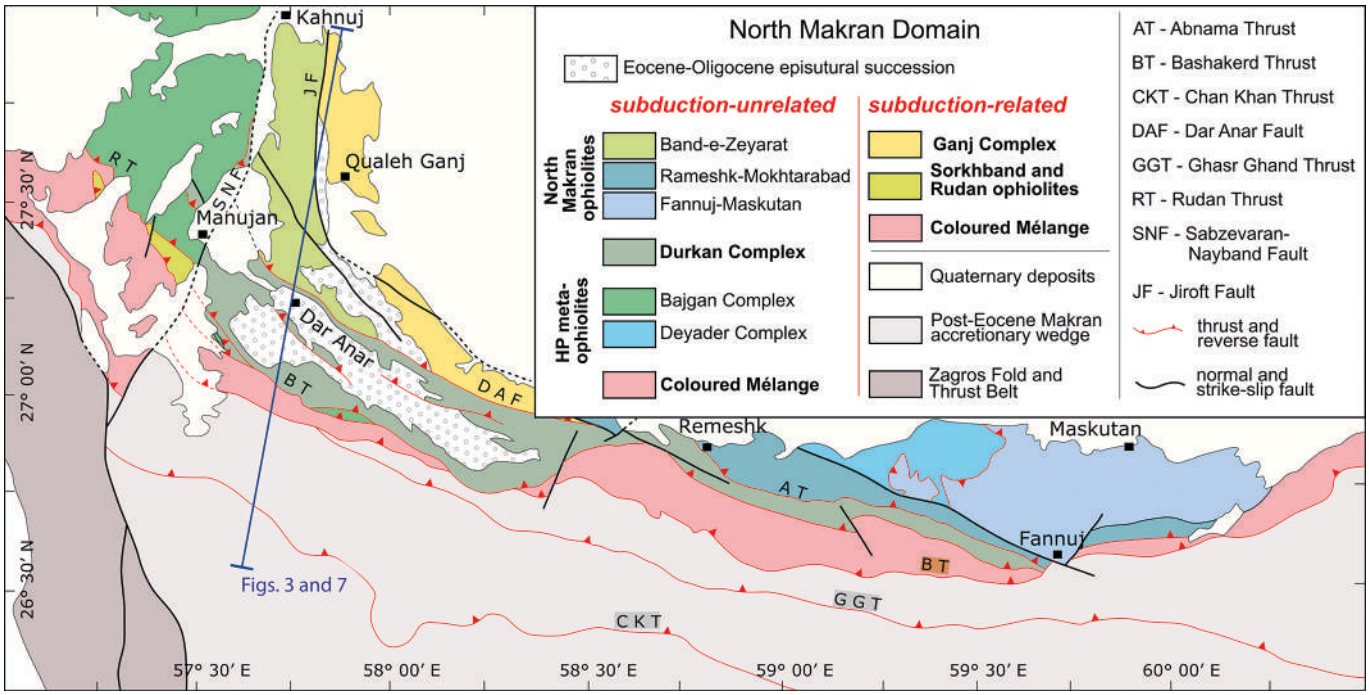

Fig. 2 - Structural scheme of the North Makran Domain. The blue line indicates the trace of the cross-section shown in Figs. 3 and 7.

THE OPHIOLITES OF THE WESTERN NORTH MAKRAN DOMAIN

In the Makran Accretionary Wedge, the ophiolites belong to the structurally innermost and uppermost tectonic domain, known as the North Makran domain after Burg et al. (2013). This domain corresponds to the backstop of the post-Eocene onshore prism that is composed of three thrust-bounded domains, namely the Inner, Outer, and Coastal Makran (Burg et al., 2013; Burg, 2018). These domains are composed of Eocene-Pleistocene mainly siliciclastic sedimentary successions, recording the sedimentation within southward-migrating and progressively younger trench and wedge-top basins (Platt et al., 1985; Dolati, 2010; Dolati and Burg, 2013; Mohammadi et al., 2016, 2017; GholamiZadeh et al., 2025a, b). Conversely, the North Makran domain comprises a tectonic assemblage of metamorphic and non-metamorphic ophiolites and ophiolitic mélanges, which are associated with deep-sea sedimentary sequences and, less frequently, trench-type turbiditic sequences (McCall and Kidd, 1982; McCall, 1985; Glennie et al., 1990; Burg, 2018; Esmaeili et al., 2020, 2021). In the North Makran domain, each tectonic unit is bounded by either high- or low-angle and south- to southwest-verging thrust zones that formed during the accretionary stage of the Neo-Tethys oceanic lithosphere (McCall, 1997; Pandolfi et al., 2021; Bröcker et al., 2021; Barbero et al., 2023b, c; Barbero et al., 2025). Southward, the mainly E-W trending Bashakerd Thrust separates the North Makran domain from the post-Eocene accretionary wedge (Burg et al., 2013). To the north, the North Makran domain is partially covered by Quaternary deposits of the Jazz Murian depression, a ~300 km wide and ~500 km long basin that represents the forearc basin of the Eocene to present-day continental volcanic arc associated with the Makran subduction (Fig. 2; Berberian et al., 1982; Delavari et al., 2022; GholamiZadeh et al., 2025a).

Several authors have investigated the metamorphic and non-metamorphic ophiolites of the North Makran domain, delineating their stratigraphy and structural architecture, their geochemical composition and petrological significance, the HP-LT metamorphic evolution, and their ages (e.g., McCall, 2002; Ghazi et al., 2004; Hunziker et al., 2015, 2017; Moslempour et al., 2015; Omrani et al., 2017; Sepidbar et al., 2020; Esmaeili et al., 2019, 2020; Barbero et al., 2020a, 2020b, 2021a, 2021b, 2023b, 2023c; Saccani et al., 2018, 2022a, 2022b; Ghasemi Siani et al., 2021; 2022a, 2022b, 2025; Pandolfi et al., 2021; Bröcker et al., 2021). According to Barbero et al. (2025), the North Makran is composed of different types of ophiolites and an ophiolitic mélange whose tectonic relationships are sealed by the unconformable deposition of late Paleocene - early Eocene sedimentary successions. The combination of the stratigraphy of the ophiolites and their sedimentary cover and the petrological features of the magmatic rocks were used to classify the North Makran ophiolites according to the integrated classification of the ophiolites and interpretation of their geodynamic setting of formation proposed by Dilek and Furnes (2011). From north to south (i.e., from the inner to the outer structural position) the ophiolites include: i) the volcanic arc type ophiolites (VA ophiolites of Dilek and Furnes, 2011) of the Ganj Complex; ii) the mid ocean ridge (MOR) type of the North Makran Ophiolites, represented by the Band-e-Zeyarat ophiolites in the western North Makran and the Remeshk-Mokhtarabad and Fannuj-Maskutan ophiolites in the central North Makran; iii) the plume-type ophiolite of the Durkan Complex; iv) the MOR-type high pressure meta-ophiolites of the Bajgan Complex in the western North Makran and the Deyader Complex in the central North Makran; v) the Sorkhband ophiolite consisting of a MOR-type ophiolite in the upper tectonic slice and a supra-subduction zone ophiolite in the lower slice (SSZ type of Dilek and Furnes, 2011); vi) the Coloured Mélange representing an ophiolitic mélange composed of slices of ophiolitic units and pelagic and trench sedimentary rocks. The ophiolitic units include both the mantle section, as well as the crustal sequence and show geochemical features typical of both subduction-related and subduction-unrelated types, including MOR-type, plume-type, and SSZ-type (Barbero et al., 2025). The Coloured Mélange is thus a tectonic mixing of fragments of the Neo-Tethys oceanic lithosphere with different age and crustal types rather than a unique section of the oceanic lithosphere (Barbero et al., 2025). In this review, we avoid discussing in detail the features of the Coloured Mélange, instead focusing on the coherent ophiolites of the North Makran domain and discussing their stratigraphic and structural characteristics and the geochemistry of the magmatic rocks within the broader context of the distinction between subduction-related and subduction-unrelated ophiolites (Dilek and Furnes, 2011). To provide a robust and well-constrained geological section across the ophiolites of the North Makran domain, this review focuses on the westernmost part of this tectonic domain (i.e., the Manujan-Kahnuj area; Fig. 2), where the structural relationships among the different tectonic units are best exposed. This allows us to define a well-grounded geological framework and to discuss the relationships between subduction-related and subduction-unrelated ophiolites.

SUBDUCTION-UNRELATED OPHIOLITES IN THE NORTH MAKRAN DOMAIN: THE TECTONO-STRATIGRAPHIC ARCHITECTURE

The subduction-unrelated ophiolites are sandwiched between the subduction-related ophiolites of the Ganj Complex, to the north, and the Sorkhband Ophiolites, to the south (see section 2.3). From the upper to the lower structural position, they show the transition from the non-metamorphic Band-e-Zeyarat Ophiolites, the partially metamorphic Durkan Complex, and the HP-LT meta-ophiolites of the Bajgan Complex (Figs. 2, 3).

Band-e-Zeyarat Ophiolites

The Band-e-Zeyarat Ophiolites include the crustal sequence of a MOR-type ophiolite (Ghazi et al., 2004; Barbero et al., 2020b, 2023c) and belong to the North Makran Ophiolites as defined by Barbero et al. (2025). The stratigraphic, structural, and geochemical data allow us to reconstruct a synthetic stratigraphic log for this unit that is well comparable with the MOR-type ophiolitic sequence (Dilek and Furnes, 2011). In fact, the Band-e-Zeyarat Ophiolites include from bottom to top ultramafic rocks, an intrusive complex, a sheeted dyke complex, a volcanic sequence, and on top of the ophiolite the pelagic sedimentary cover (Figs. 3a, 4a-c). The ultramafic rocks include plagioclase-bearing lherzolite, clinopyroxene-bearing harzburgite, dunite, plagioclase-dunite, and podiform chromitite, likely representing lower oceanic crustal cumulate rather than mantle peridotite (Fig. 4; Arvin et al., 2005; Kananian et al., 2001; Ghazi et al., 2004; Barbero et al., 2020b, Ghasemi Siani et

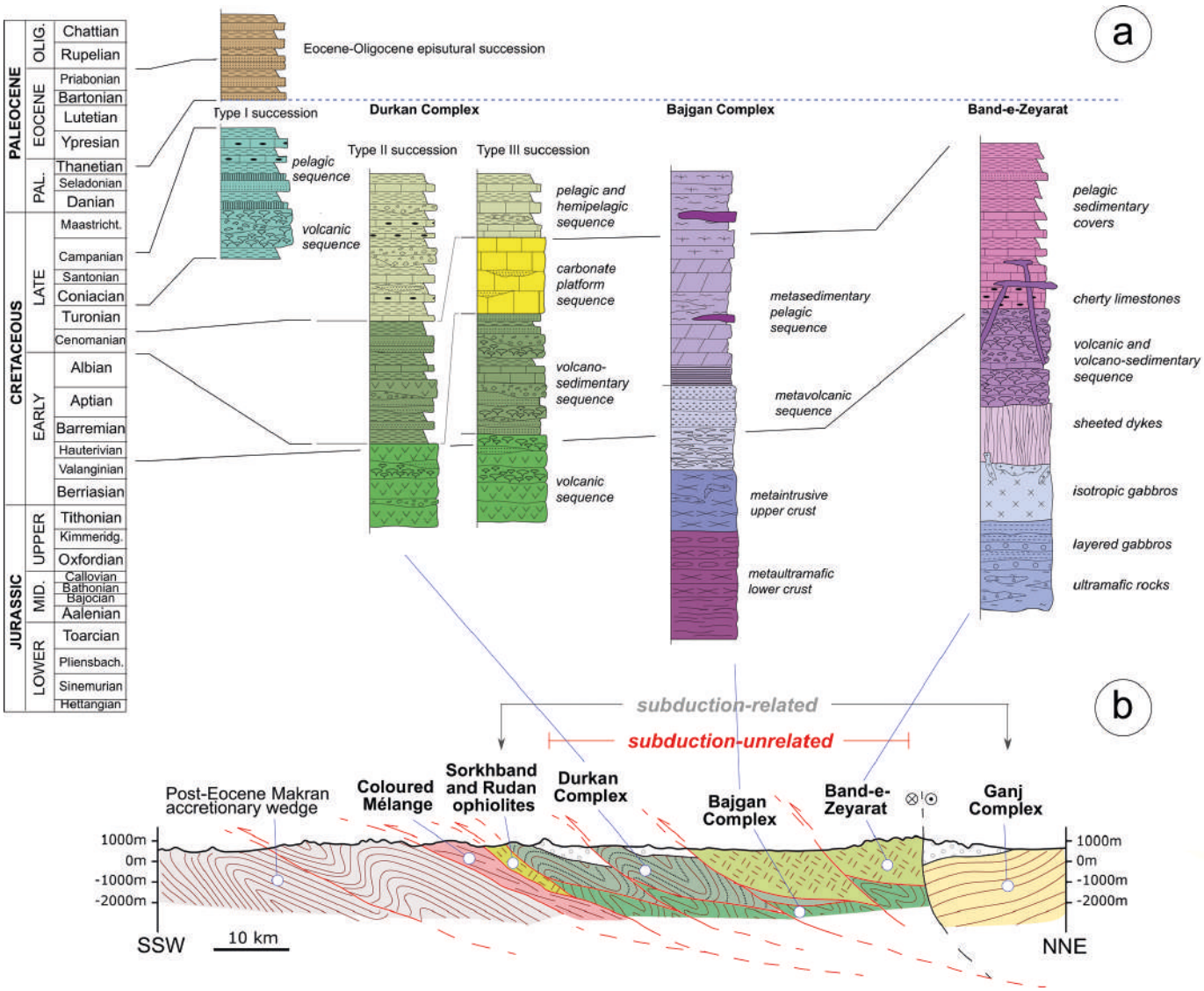

Fig. 3 - a) Lithostratigraphic columns of the subduction-unrelated tectonic units of the North Makran Domain and b) simplified geological cross-section (see Fig. 2 for its location).

al., 2021, 2022a, 2025). The intrusive complex is composed of a lower part with layered rocks followed by an upper part with isotropic intrusive rocks. The lower layered part shows cm- to m-scale magmatic layering defined by the alternation of olivine gabbro, troctolite, pegmatitic olivine gabbro, anorthosite, and wehrlite (Fig. 4a). Gabbro commonly displays a strong magmatic foliation defined by aligned plagioclase and pyroxene. The upper isotropic part is dominated by isotropic gabbro, ferrogabbro, and diorite, intruded by small plagiogranite bodies and dykes. Plagiogranite and basaltic dykes (Fig. 4b) are particularly abundant at the top of this complex, near the transition to the sheeted dykes. Various lithologies from the intrusive complex have been dated since the 1980s with different radiometric techniques (see Barbero et al., 2025 for details). The results of these radiometric datings indicate ages ranging from 146 ± 5 Ma to 122 ± 2 Ma (Hassanipak et al., 1996; Ghazi et al., 2004; Barbero et al., 2020b; Ghasemi Siani et al., 2021). The overlying sheeted dyke complex consists of parallel to sub-parallel doleritic dykes ranging from 10 cm to 3 m in thickness. This complex is followed by a volcanic sequence through a transitional zone of pillow and massive lavas intruded by frequent sills and dykes. Pillow lavas and massive lavas are interlayered with pillow breccia, which contain fragments of pillow basalt, pelagic limestone, and chert within a glassy matrix (Fig. 4c). Upward, lava flows are interlayered with thin, discontinuous marls and limestone affected by soft-sediment deformation, indicating emplacement onto poorly consolidated sediments. The Band-e-Zeyarat Ophiolites are capped by Hauterivian-Cenomanian pelagic sedimentary cover that, from bottom to top, consists of cherty limestone, alternating marls and limestones, and varicoloured marls with intercalation of volcaniclastic arenite with particularly abundant lithic fragments of quartz-rich volcanic rocks. Age constraints were obtained with nannoplankton biostratigraphy by Barbero et al. (2023c). The lower part of the sedimentary cover is intruded by basaltic sills and dykes.

From the structural point of view, the Band-e-Zeyarat Ophiolites represent a mainly N-S oriented tectonic element separated from the Ganj Complex and the Bajgan Complex by the N-striking Jiroft Fault and the NNE- striking Sabzevaran-Nayban Fault, respectively (Figs. 2, 3b). Southward these ophiolites are thrust over the Durkan Complex. Internally, the Band-e-Zeyarat Ophiolites are composed of different tectonic

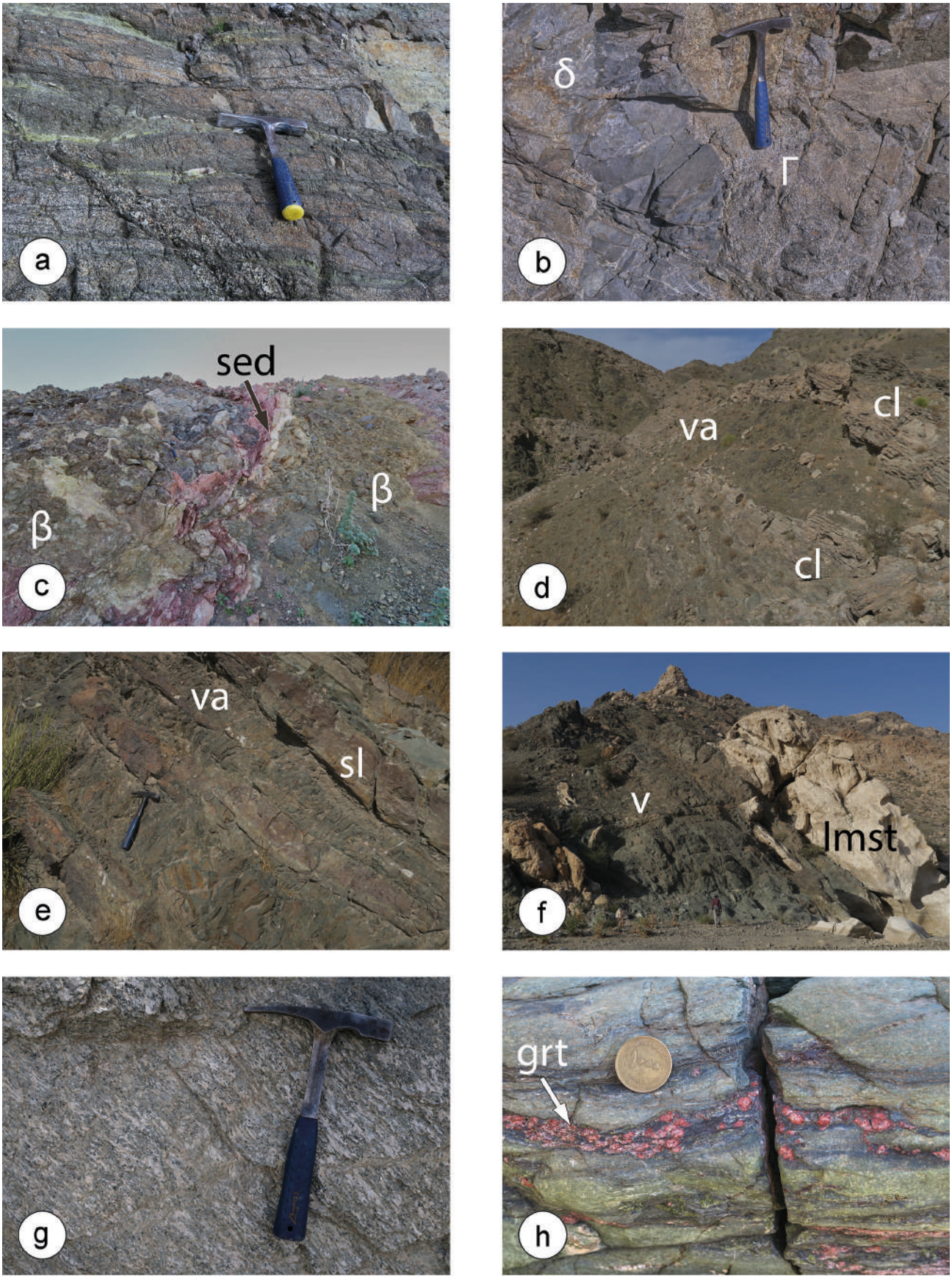

Fig. 4 - Field occurrence of the subduction-unrelated ophiolites from the Band-e-Zeyarat, Durkan, and Bajgan ophiolites and metaophiolites. Band-e-Zeyarat ophiolite: a) layered gabbro; b) fine grained gabbro (Γ) from the isotropic facies crosscut by a doleritic basaltic dyke (δ); c) pillow lavas and pillow breccia basalts (β) interlayered with pelagic limestones and red siliceous marls (sed). Durkan Complex: d) Type-I succession, deep water cherty limestones (cl) interlayered with volcaniclastic arenites (va); e) Type-II succession, deep water silty limestones (sl) interlayered with volcaniclastic arenites (va); f) Type-III succession, volcanic rocks and volcaniclastic arenites (v) interlayered with massive platform limestone (lmst) indicating a shallow-marine depositional setting. Bajgan Complex: g) highly deformed metagabbro; h) garnet (grt)-bearing metabasalt.

slices bordered by N-S oriented high-angle faults. The structural setting is mainly characterized by sub-isoclinal to tight folds re-deformed by open to tight folds with sub-horizontal axial planes (Barbero et al., 2023c for further details). These folding stages were achieved during the incorporation of the ophiolite within the accretionary prism and the subsequent exhumation. The sub-isoclinal to tight folds are associated with an axial planar foliation (Fig. 5a) indicating deformation at shallow structural level (Barbero et al., 2023c for further details). In fact, this foliation is represented by a weak pressure solution cleavage within the marls without any metamorphic recrystallization, and a radial fanning disjunctive cleavage in the limestones (Fig. 5b). A late Paleocene - early Eocene sedimentary succession unconformably rests onto the deformed Band-e-Zeyarat Ophiolites, indicating its accretion and deformation in the prism before the late Paleocene (Barbero et al., 2023c).

Durkan Complex

Traditionally, the Durkan Complex was interpreted as the sedimentary cover of a continental margin (McCall and Kidd, 1982; Hunziker et al., 2015), but recent multidisciplinary studies demonstrate it is composed of fragments of a Late Cretaceous oceanic seamount chain disrupted during subduction-related processes (Barbero et al., 2021a, b, 2023b). The age constraints were derived from an integrated biostratigraphic study, combining radiolarian, nannoplankton, and foraminifera biostratigraphy (see Barbero et al., 2021a for details). The Durkan Complex consists of multiple tectonic slices. These slices show coherent stratigraphic successions, showing either no-metamorphic overprint or blueschist facies metamorphic signatures (Barbero et al., 2021a, 2023b). In the Manujan area, Barbero et al. (2021a) distinguished three main succession types (Type-I-III), all including meta-igneous and meta-sedimentary lithologies as well as magmatic and sedimentary rocks, all derived from different seamount settings (Figs. 3a, 4d-f). To focus on the description of the stratigraphy in each seamount setting, in the following we use the sedimentary rocks nomenclature since the pristine stratigraphic succession is still preserved even in the strongly metamorphosed tectonic slices. Type-I succession formed in deep-water marine environment testified by the alternation of thin-bedded red chert, cherty limestone, shale, shaly marl, and pillow basalt along with minor volcaniclastic arenite and pillow breccia (Fig. 4d). This succession represents the deep-water developmental stage of a seamount, characterized by pelagic sedimentation and volcanic activity (Barbero et al., 2021a). Type-II succession is composed of a volcanic sequence passing upward to a volcano-sedimentary sequence, in turn, followed by a pelagic to hemipelagic succession. Massive lava flows, pillow lavas, and volcaniclastic arenite and breccia are particularly abundant in the volcanic and volcano-sedimentary sequence. In the latter, shale and limestone increase in abundance upward and are intercalated with mixed carbonate and volcaniclastic breccia and/or arenite (Fig. 4e). Upward, the pelagic to hemipelagic succession comprises cherty limestone, shale, chert, and minor carbonate breccia and volcaniclastic arenite. The limestone in the Type-II succession bears pelagic foraminifera indicative of sedimentation in relatively deep-water environment. Overall, Type-II records sedimentation along and at the base of a seamount flank during the shallow-water shield stage of seamount growth (Barbero et al., 2021a). Type-III succession differs mainly from the Type-I and -II because shallow-marine carbonate platform rocks are associated with the volcanic and volcano-sedimentary sequences. The volcanic sequence includes alternating pillow and massive lavas with volcaniclastic arenites. The volcano-sedimentary sequence is different as it contains volcanic rocks mixed with volcaniclastic arenites and breccias, shales, mixed carbonate-volcanic turbidites, and locally, platform-derived massive limestones indicating a shallow-marine depositional setting (Fig. 4f). The carbonate platform succession contains massive limestones and subordinate volcaniclastic arenites, with no evidence of lava flows. The Type-III succession ends upward with a hemipelagic and pelagic sequence. The stratigraphic features of the Type-III succession testify to shallow-water volcanic activity and carbonate platform development atop a seamount summit during its shallow-water growth stage.

Structurally, the Durkan Complex in the Manujan area defines an ESE-WNW trending belt sandwiched between the Band-e-Zeyarat Ophiolites and the Bajgan Complex (Figs. 2, 3b). However, the Bajgan Complex is generally completely cut off along the thrust zones, and the Durkan Complex is directly juxtaposed to the Coloured Mélange. The thrust-bounded structural stack is crosscut by the NNE-striking dextral Sabzevaran-Nayban Fault. The structural evolution (Figs 5c, d) reflects underplating under blueschist-facies conditions followed by exhumation to shallower levels within an accretionary prism (Barbero et al., 2023b). In fact, a first phase of deformation characterized by sub-isoclinal to tight folds associated with reverse shear zones along the overturned limb is representative for the underplating of the seamount fragments at the base of the accretionary prism. This is further constrained by the thermodynamic modelling on the metamorphic paragenesis of the axial planar foliation, which testifies the deformation within blueschist-facies condition at P = 0.6 - 1. GPa and T = 160 - 310 °C (Barbero et al., 2023b). These folds are re-folded by open to tight folds with axial planar foliation forming a crenulation cleavage in the shale and a disjunctive cleavage in the competent lithologies such as marble and meta-arenite. The lack of metamorphic recrystallization associated with this foliation indicates the deformation at shallower structural level with respect to the blueschist-facies event. This indicates the deformation during the progressive exhumation of the Durkan Complex. These structures are unconformably sealed by late Paleocene-Eocene turbidite succession.

Bajgan Complex

In the literature, the Bajgan Complex was considered as a Paleozoic (or older) metamorphic basement of a continental microplate (McCall and Kidd, 1982; Dorani et al., 2017), but recent work has demonstrated unequivocally that the Bajgan Complex consists of Late Jurassic to Early Cretaceous meta-ophiolites and associated meta-sedimentary sequences, all affected by HP-LT metamorphism during the Late Cretaceous (Pandolfi et al., 2021). The age data for the magmatic emplacement of the ophiolitic gabbro were derived from U/Pb zircon dating, whereas the age data for the HP-LT metamorphism are based on Ar/Ar dating of metamorphic white mica from micaschist from the sedimentary cover (see Pandolfi et al., 2021 and details therein). These findings led to the classification of the Bajgan Complex as high-pressure meta-ophiolites as defined by Barbero et al. (2025), interpreting it as the remnants of a subduction complex composed of deformed and metamorphosed fragments of oceanic lithosphere and sedimentary cover.

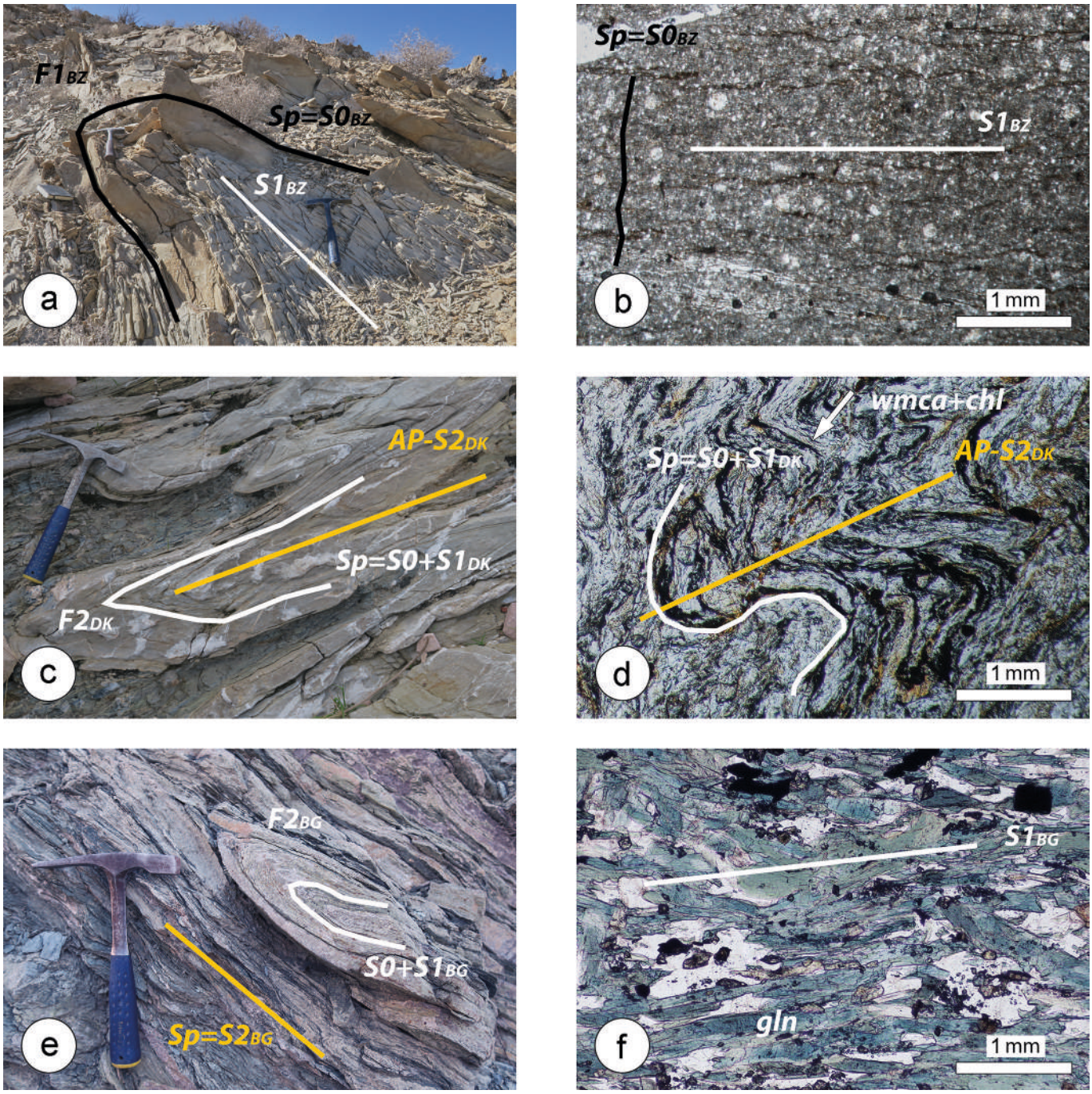

Fig. 5 - The figure highlights the different metamorphic and deformational features observed in the Band-e-Zeyarat (BZ), Durkan (DK) and Bajgan (BG) units, at both outcrop and microscopic scales. The abbreviation *Sp* denotes the main surface recognizable at the mesoscale. *Band-e-Zeyarat Unit:* (a) F1 fold and associated axial-plane foliation S1 within the carbonate sedimentary cover; (b) detail of the S1 axial-plane foliation, expressed as a pressure-solution surface. *Durkan Complex*: (c) F2 fold with associated axial-plane foliation AP-S2. The composite surface defined by bedding and S1 foliation is indicated as (S0+S1); (d) micro-scale detail of the F2 hinge zone. The composite surface S0+S1, characterized by the crystallization of white mica and chlorite (wmca + chl), is folded by the subsequent D2 phase, whose axial plane AP-S2 is clearly visible. *Bajgan Ophiolite*: (e) F2 fold developed from reworking of the composite surface S0+S1. The main surface visible at outcrop scale is the S2 foliation; (f) micro-scale detail of the S1 foliation, characterized by the growth of blue amphibole (gln).

The Bajgan Complex is composed of several tectonic slices that collectively form a reconstructed crustal section of oceanic lithosphere, for which a synthetic stratigraphic log has been proposed integrating field observations in several outcrops (Figs. 3a, 4g-h; Barbero et al., 2025). From bottom to top, the Bajgan Complex stratigraphy includes the serpentinite, the meta-intrusive, the meta-volcanic rocks, and the meta-sedimentary succession. Serpentinites likely represent the former ultramafic cumulates from the lower oceanic crust. They are associated with meta-intrusive rocks derived from the deformation and metamorphism of anorthosite, melagabbro, and gabbro (Fig. 4g) with minor plagiogranite. The meta-volcanic rocks include amphibolite and blueschist derived from the metamorphism of massive and pillow basaltic lavas (Fig. 4h). The meta-sedimentary cover is composed of quartzite, marble, micaschist, calcschist, and paragneiss.

These lithologies derive from deep-sea pelagic sediments such as chert, limestone, and turbidite, documenting the evolution of the oceanic domain prior to subduction.

Structurally, the Bajgan Complex is widely exposed in the Manujan area, extending between the Sabzevaran Fault to the east and the Rudan Thrust to the south (Fig. 2). In this area, it is tectonically covered by the Durkan Complex and is thrust over the subduction-related Sorkhband Ophiolites and the Coloured Mélange (Fig. 3b). The Bajgan Complex consists of multiple tectonic slices separated by NW-SE trending mylonitic shear zones. Internally, each slice shows well-developed NW-SE trending foliation. A multiscale structural analysis highlights a polyphase deformation history achieved during the progressive underplating at the base of the Makran subduction Complex followed by its exhumation at shallower structural levels (Pandolfi et al., 2021). The underplating stages are testified by two deformation phases (D1 and D2, Fig. 5e), recording a prograde metamorphic evolution. The D1 structures consist of structural relicts in low-strain domains and consists of S1 foliation (Fig. 5f) and rootless isoclinal folds formed during the early stage of the underplating and the prograde metamorphism. The white mica+chlorite+albite+quartz mineral assemblages within S1 constrain peak blueschist-facies conditions of ~250-295 °C and ~0.52-0.94 GPa, corresponding to burial depths of ~17-31 km (Pandolfi et al., 2021). The D2 structures (Fig. 5e) are the most common and well-preserved in the outcrops and consist of tight to isoclinal folds as well as shear zones with S-SW shearing sense. The associated S2 axial planar foliation forms a pervasive schistosity from meso- to micro-scale. Thermobarometric calculations based on the equilibrium of mica+chlorite+albite+quartz grew along the S2 foliation indicate that this foliation developed along a retrograde path, with early D2 conditions of ~450 °C and ~0.80-1.10 GPa, followed by late D2 at ~315-350 °C and ~0.28-0.57 GPa (Pandolfi et al., 2021). D2 structures reflect deformation within the subduction channel at the peak conditions, immediately before the beginning of the exhumation stages (see Pandolfi et al., 2021 for further details). The complete exhumation of the Bajgan Complex has been achieved with close to open folds with sub-horizontal axes associated with a crenulation cleavage and with open to gentle folds with no syn-kinematic metamorphic recrystallization.

SUBDUCTION-UNRELATED OPHIOLITES IN THE NORTH MAKRAN DOMAIN: GEOCHEMICAL AND PETROGENETIC FEATURES

The Band-e-Zeyarat Ophiolite

The geochemical characteristics and petrogenetic constraints of the Band-e-Zeyarat magmatic rocks summarized in this section are based on data previously reported by Barbero et al. (2020a). Volcanic and subvolcanic rocks of the Band-e-Zeyarat Ophiolites are mainly represented by basalt, with subordinate basaltic andesite, andesite, Fe-basalt, and very rare rhyolitic dykes. These lithologies occur as individual dykes intruding the intrusive complex, dolerite forming the sheeted dyke complex, and basaltic lavas in the volcanic sequence. No systematic geochemical differences are observed among these units, indicating that they represent products of the same magmatic system at different structural levels. Consequently, they are described together regardless of their stratigraphic position.

All volcanic and subvolcanic rocks display variable but generally low Nb/Y ratios (0.08 - 0.13), indicating a sub-alkaline affinity. Major element compositions are highly variable, reflecting melts at different stages of magmatic differentiation (e.g., CaO = 2.1 - 12.5 wt%, Al_2O_3 = 11.4 - 18.4 wt%, MgO = 1.2 - 14.4 wt%, TiO_2 = 0.35 - 3 wt%, P_2O_5 = 0.06 - 0.54 wt%, Mg# = 76 - 41). Covariation trends of Al_2O_3/TiO_2 versus Ti indicate fractional crystallization dominated by olivine, followed by plagioclase, plagioclase + clinopyroxene, and finally magnetite. These features, together with the low Nb/Y ratios, indicate a common tholeiitic evolutionary trend for the volcanic and subvolcanic rocks of the sheeted dyke complex and volcanic sequence.

Despite this overall coherence, incompatible trace element and REE (rare earth elements) systematics allow the distinction of two main geochemical types: N-MORB (normal-type mid-ocean ridge basalts) and E-MORB (enriched-type mid-ocean ridge basalts), both of which occur in the volcanic sequence and the sheeted dyke complex; however, E-MORB rocks are generally more abundant than N-MORB rocks toward the upper part of the volcanic sequence.

N-MORB-type basalts

N-MORB rocks include basalts and rhyolitic dykes. The basalts exhibit very low Nb/Y ratios (0.08-0.11) and low abundances of Y (15.0 - 50.7 ppm), Zr (55.4 - 143 ppm), Nb (1.36 - 5 ppm), Th (0.063 - 0.611), Ta (0.090 - 0.440 ppm), and LREE (light REE). Their N-MORB-normalized incompatible element patterns are relatively flat (Fig. 6a), with low overall abundances of HFSE (high field strength elements) and LILE (large ion lithophile elements) and only minor Ti anomalies. Chondrite-normalized REE patterns are flat from MREE (medium REE) to HREE (heavy REE), whereas LREE are variably depleted relative to MREE, as indicated by low $(La/Sm)_N$ (0.34-0.9) and $(La/Yb)_N$ (Fig. E1b) ratios and near-unity $(Sm/Yb)_N$ values. Minor positive or negative Eu anomalies are locally observed.

These geochemical features closely match those of typical N-MORB derived from depleted MORB mantle sources. In the tectonic discrimination diagram of Saccani (2015), these basalts plot close to the N-MORB field (Fig. 6c), supporting a subduction-unrelated mid-ocean ridge origin. The rhyolitic dykes display high incompatible element contents and a pronounced negative Eu anomaly, reflecting advanced fractional crystallization dominated by plagioclase removal. Their REE and trace element characteristics indicate derivation from differentiation of N-MORB-like parental melt.

E-MORB-type

E-MORB rocks consist mainly of basalt with subordinate basaltic andesite and andesite and are distinguished by higher Nb/Y ratios (0.14-0.42) and systematically higher Nb (3.59-19.46 ppm), Zr (72.3 - 340 ppm), Th (0.22 - 1.31 ppm), Ta (0.18 - 1.07 ppm), Y (17.8 - 78.2 ppm), and LREE contents than N-MORBs. Their N-MORB-normalized incompatible element patterns show enrichment of LILE relative to HFSE and smoothly decreasing trends from Th to Y (Fig. 6a), closely resembling those of the typical E-MORB composition (Sun and McDonough, 1989). Negative Ti anomalies occur in some differentiated samples, reflecting fractionation of Fe-Ti oxides. Chondrite-normalized REE patterns show overall enrichment of LREE relative to MREE and HREE with $(La/Yb)_N$ = 1.3 -3.1 and $(La/Sm)_N$ = 1.2 - 1.9, although individual samples display cross-cutting patterns (Fig. 6b). E-MORB rocks from the Band-e-Zeyarat Ophiolites plot in the field for

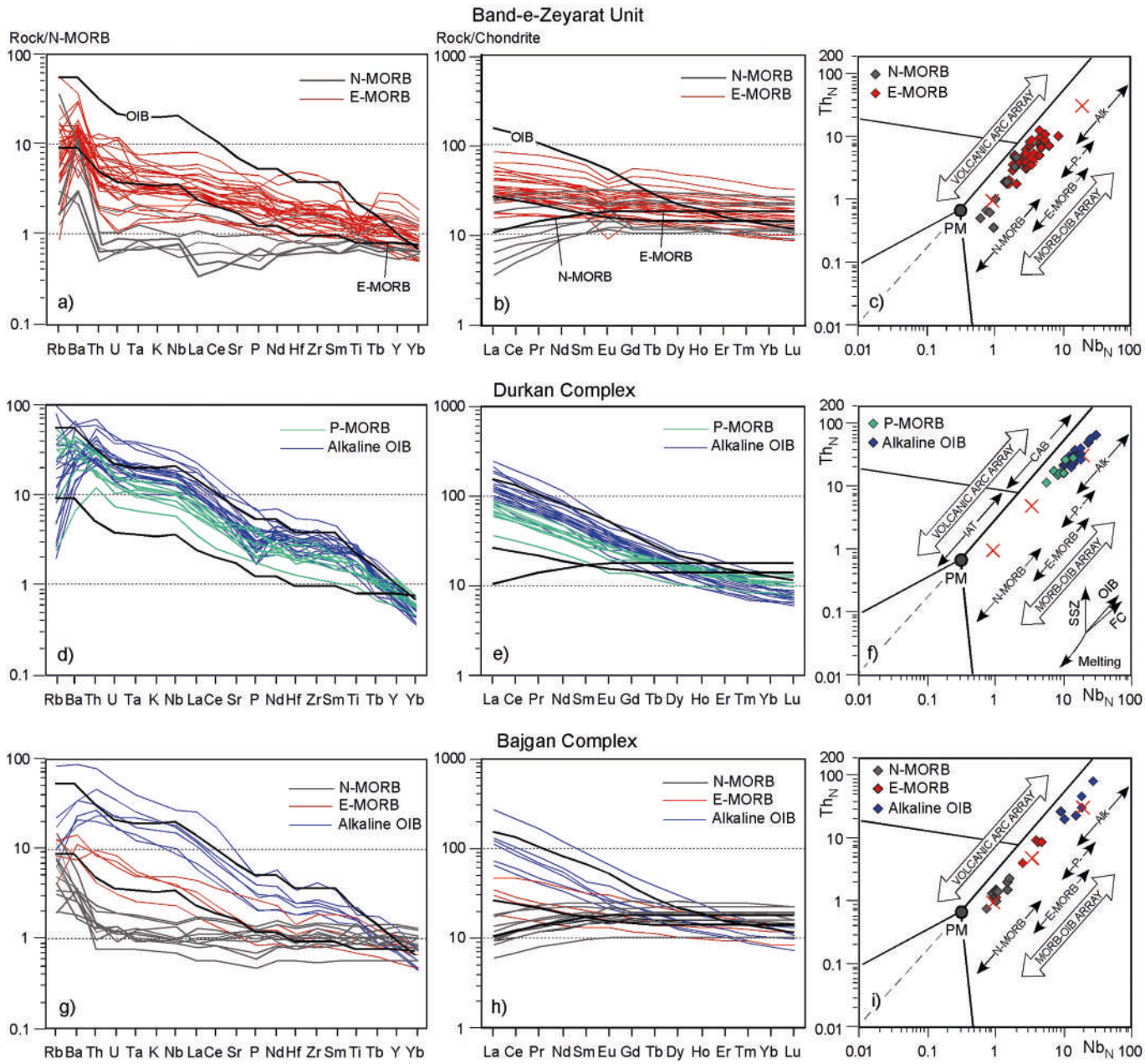

Fig. 6 - N-MORB normalized incompatible element patterns (left column), Chondrite-normalized rare earth element (REE) patterns (central column), and N-MORB normalized Th vs. Nb discrimination diagrams of Saccani (2015) (right column) for subvolcanic, volcanic, and metavolcanic rocks from the subduction-unrelated ophiolites and meta-ophiolites from the North Makran domain. Normalizing values are from Sun and McDonough (1989). Black lines in the extended incompatible element diagrams and red crosses in the Th-Nb diagrams indicate the composition of normal (N-MORB) and enriched (E-MORB) mid-ocean ridge basalts, as well as alkaline ocean island basalt (OIB). Normalizing values from Sun and McDonough (1989). Vectors in the Th-Nb diagrams indicate the trends of compositional variations due to the main petrogenetic processes (OIB: plume-type-component enrichment; FC: fractional crystallization; SSZ: supra-subduction zone component enrichment). Arrows broadly indicate the compositional variation of N-MORBs, E-MORBs, plume-type MORBs (P-), and alkaline basalts (alk) data from Saccani (2015).

subduction-unrelated settings, within the compositional field for rocks with E-MORB affinity in the discrimination diagram in Fig. 6c.

Variations in REE contents reflect magmatic differentiation from parental melts with slightly different compositions, related to partial melting of heterogeneous mantle sources under variable conditions (Allègre and Minster, 1978). Although differences are minor, Barbero et al. (2020a) identified distinct rock subtypes based on REE characteristics. Some basalts show gently sloping REE patterns, high Ta/Hf and Th/Nb ratios, and marked negative Eu anomalies indicating plagioclase fractionation. Others display steeper LREE/HREE patterns, stronger LREE enrichment, variable Eu depletion, and lower Ta/Hf and Th/Nb ratios. Additional variants range from nearly flat REE patterns to strongly LREE-enriched compositions with minor Eu anomalies, higher Nb and Th contents, and elevated Nb/Y and Zr/Nb ratios. Overall, although these geochemical differences are subtle, they suggest variations in mantle source enrichment and melting conditions rather than being controlled solely by fractional crystallization processes (Barbero et al., 2020a).

Petrogenetic implications

The volcanic and subvolcanic rocks of the Band-e-Zeyarat Ophiolites record magmatism typical of subduction-unrelated oceanic settings (Fig. 6c) and are dominated by tholeiitic melts with N-MORB and E-MORB affinities. N-MORB-type rocks derived from partial melting of a depleted MORB mantle with negligible plume-type enrichment, whereas E-MORB-type rocks formed from variably enriched mantle sources influenced by OIB-type (within-plate ocean island basalts) components. Petrogenetic modelling indicates that differences among E-MORB compositions reflect a combination of variable degrees of mantle enrichment, partial melting, and melting depths. Together with data from intrusive rocks and other North Makran Ophiolites (Ghazi et al., 2004; Hunziker, 2014; Barbero et al., 2020b, Saccani et al., 2022a), these results suggest that the Band-e-Zeyarat Ophiolites represent part of a chemically composite oceanic crust formed during the Early Cretaceous. This crust records incipient mantle plume activity and variable plume-ridge interaction during the evolution of the Neo-Tethyan oceanic lithosphere.

The Durkan Complex

The magmatic rocks of the Durkan Complex are dominated by basalts and ferrobasalts, with subordinate basaltic andesites and rare evolved compositions including trachyte and alkali rhyolite. These rocks occur with variable degrees of deformation and metamorphic overprinting; however, metavolcanic rocks are discussed together with their unmetamorphosed counterparts, as the geochemical characteristics of the original volcanic protoliths do not relate to the later tectono-metamorphic processes. For simplicity, the prefix "meta" is omitted hereafter. The geochemical characteristics and petrogenetic constraints of the Durkan magmatic rocks summarized in this review were originally presented by Barbero et al. (2021b).

Basaltic rocks show wide variations in major and trace element compositions, indicating derivation from melts generated at different degrees of partial melting and magmatic differentiation. Based on Nb/Y ratios (Pearce, 1996), two main geochemical rock types have been distinguished by Barbero et al. (2021b). P-MORB (plume-type mid-ocean ridge basalts) rocks display transitional affinities with Nb/Y ratios between ~0.7 and 1.0, whereas alkaline OIB rocks exhibit a clear alkaline affinity, with Nb/Y ratios generally >1 and locally reaching values up to ~4.

P-MORB-type volcanics

P-MORB-type volcanics include basalts, basaltic andesites, ferrobasalts and one trachyte sample. These rocks are predominantly associated with the Type-I succession, are less common in the Type-II succession, and are absent in the Type-III succession. The basalts display a broad compositional range (SiO_2 = 43.3 - 53.3 wt%, MgO = 4.9 - 11.9 wt%, Al_2O_3 = 12.2 - 17.2 wt%, Mg# = 48-75), suggesting variable degrees of fractionation. They are characterized by relatively high TiO_2 (1.20-2.29 wt%) and P_2O_5 (0.23-0.51 wt%) contents, enrichment in incompatible elements such as Zr (73-220 ppm), Nb (13.5-32.6 ppm), Th (1.49-3.66 ppm), and Ta (0.92-2.18 ppm) contents, coupled with comparatively low Y abundances (16.9-33.5 ppm). Compatible elements (Cr, V, Ni, Co) show variable but generally high contents, consistent with basaltic compositions. Ti/V ratios (28-61) fall within the range typical of MORB to transitional alkaline basalts (Shervais, 1982). N-MORB-normalized incompatible element patterns display smoothly decreasing trends from Th to Yb, with significant enrichment of Th, Ta, and Nb relative to Yb (Fig. 6d), as indicated by high $(Th/Yb)_N$, $(Ta/Yb)_N$, and $(Nb/Yb)_N$ ratios. Chondrite-normalized REE patterns show mild LREE enrichment relative to HREE and moderate HREE depletion relative to MREE (Fig. 6e), with $(La/Yb)_N$ = 4.4-7.9 and $(Sm/Yb)_N$ = 1.2-3.2. Overall, the geochemical features of the Durkan P-MORB rocks closely resemble those of plume-type MORB (P-MORB) erupted in modern mid-ocean ridge settings influenced by mantle plume activity (e.g., Le Roex et al., 1983). In tectonic discrimination diagrams, these rocks plot within subduction-unrelated oceanic fields between typical P-MORB and alkaline basalt compositions (Fig. 6f).

The trachyte is distinguished by high SiO_2 and low MgO contents, very high Zr and Y contents, and strong depletion in compatible elements, TiO_2, and P_2O_5, reflecting advanced magmatic differentiation. Its geochemical signatures include pronounced negative Ti and P anomalies in N-MORB-normalized patterns and a strong negative Eu anomaly in REE patterns (Figs. 6d, e), consistent with early fractionation of plagioclase, Fe-Ti oxides, apatite, and amphibole.

Alkaline OIB-type

Alkaline OIB-type rocks predominantly comprise basaltic and ferrobasaltic rocks and very minor alkali rhyolites. These rocks are mainly found in the Type-II and Type-III successions and are absent in the Type-I succession. Basalts in this group display variable SiO_2 contents (41.9 - 53.5 wt%) and Mg# values (39 - 75), indicating melts formed at different stages of differentiation. These basalts are enriched in TiO_2 (1.55 - 5.13 wt%), P_2O_5 (0.20 - 1.10 wt%), Zr (139 - 403 ppm), Nb (23.6 - 71.8 ppm), and Ta (1.42 - 5.13 ppm), while Y contents (18.5 - 33.0 ppm) remain relatively low. High Ti/V ratios (41 - 76, Shervais, 1982), elevated Ti/Y (526-1448) and Zr/Y (6.7-20.6) ratios and strongly enriched incompatible element patterns distinguish them from P-MORB rocks. N-MORB-normalized spider diagrams show pronounced enrichment in Nb and Ta relative to Yb (Fig. 6d), with very high $(Th/Yb)_N$, $(Ta/Yb)_N$, and $(Nb/Yb)_N$ ratios. Chondrite-normalized REE patterns are characterized by strong LREE/HREE and MREE/HREE enrichment (Fig. 6e), with $(La/Yb)_N$ = 9-28 and $(Sm/Yb)_N$ = 3.5-8.4, reflecting significant HREE depletion. The alkali rhyolites show geochemical features typical of highly evolved alkaline magmas, including very high Zr and Y contents, strong negative Ti, P, and Eu anomalies, and depletion of HREE relative to both LREE and MREE. The overall geochemical characteristics of alkaline rocks closely resemble those of within-plate alkaline volcanic rocks typical of oceanic islands (OIB, Sun and McDonough, 1989). In tectonic discrimination diagrams, these samples plot within the field of subduction-unrelated alkaline basalts and cluster around OIB compositions (Fig. 6f).

Despite similar major and trace element contents at comparable degrees of differentiation, Barbero et al. (2021b) further subdivided the Durkan alkaline basalts into two groups based on systematic differences in REE patterns and selected trace element ratios. These variations are independent of magmatic differentiation and instead reflect differences in mantle source characteristics and melting conditions.

Petrogenetic and tectonic implications

Petrogenetic modelling based on REE and incompatible elements, such as Th, Nb, Zr, Y, and TiO_2 (Barbero et al.,

2021b) suggests that both P-MORB-type and alkaline basalts of the Durkan Complex were generated by partial melting of a depleted sub-oceanic mantle source that was variably metasomatized by OIB-type (plume-related) components. The geochemical differences between Group 1 and Group 2 rocks can be explained by variations in the degree of plume-related enrichment, partial melting extent, and melting depth within spinel- and garnet-facies mantle domains. These geochemical data collectively indicate that the oceanic lithosphere on which the Durkan volcanic edifices developed was influenced by significant mantle plume activity in a within-plate oceanic setting during the Late Cretaceous.

The Bajgan Complex

Despite the intensive deformation and metamorphic overprinting, metavolcanic rocks are described in this section in terms of their original volcanic protoliths, as the present study focuses on their geochemical characteristics and tectono-magmatic significance, irrespective of later tectono-metamorphic modifications. For clarity, the prefix "meta" is omitted throughout the text. The main geochemical features and petrogenetic constraints of the Bajgan magmatic rocks discussed in this section are derived from Pandolfi et al, (2021) and Saccani et al. (2024).

The metavolcanic rocks investigated in the Bajgan Complex are basaltic in composition, with SiO_2 contents ranging from 42.6 to 51.8 wt% and MgO from 7.3 to 11.8 wt%. Mg# values span a relatively wide range (53 - 70), but most samples display high Mg#, indicating that the basaltic protoliths generally represent weakly evolved melts. The estimated degree of magmatic fractionation is modest, on the order of ~10-30%. Based on incompatible trace element systematics and REE distributions, the basaltic protoliths can be subdivided into distinct geochemical types corresponding to N-MORB, E-MORB, and alkaline (OIB-type) affinities, consistent with previous studies on the Bajgan Complex.

N-MORB-type basalts

N-MORB-type protoliths are sub-alkaline basalts characterized by relatively high TiO_2 (1.10-1.80 wt%) coupled with low P_2O_5 (0.07-0.16 wt%), and Nb (1.85-3.66 ppm). They display very low Nb/Y (0.07 - 0.15) and Nb/Yb (0.7 - 1.06) ratios. N-MORB-normalized incompatible element patterns are flat, with no significant enrichment of Th, Ta, or Nb relative to Yb (Fig. 6g), as indicated by low $(Th/Yb)_N$, $(Ta/Yb)_N$, and $(Nb/Yb)_N$ ratios generally close to unity. Chondrite-normalized REE patterns show depletion of LREE relative to MREE and HREE (Fig. 6h), with low $(La/Sm)_N$ (0.53-0.79) and $(La/Yb)_N$ (0.51-0.81) ratios and near-unity $(Sm/Yb)_N$ (0.96-1.10) values. These features are typical of normal mid-ocean ridge basalts generated from a depleted mantle source and are consistent with formation in subduction-unrelated ridge settings, as further supported by their position in the Th-Nb tectonic discrimination diagram, where they plot within the subduction-unrelated N-MORB field (Fig. 6i; Saccani, 2015).

E-MORB-type basalts

E-MORB-type protoliths are also sub-alkaline basalts but differ from N-MORBs by higher Nb/Y ratios (0.35-0.45) and systematic enrichment in incompatible elements, including P_2O_5 (0.15-0.31 wt%), Nb (8.99-11.4 ppm), Ta (0.67-0.76 ppm), Th (1.04-1.17 ppm), and LREE. Their N-MORB-normalized incompatible element patterns display smoothly decreasing trends from Th to Yb, with moderate enrichment of Th, Ta, and Nb relative to Yb (Fig. 6g). Chondrite-normalized REE patterns show slight LREE enrichment relative to MREE and HREE (Fig. 6h), with elevated $(La/Sm)_N$ and $(La/Yb)_N$ ratios compared to N-MORBs, and $(Sm/Yb)_N$ values indicating moderate MREE/HREE fractionation. These geochemical features closely resemble those of enriched MORB as defined by Sun and McDonough (1989) and indicate derivation from a mantle source that experienced limited enrichment relative to a depleted MORB mantle.

Alkaline (OIB-type) basalts

Alkaline basaltic protoliths display a clear alkaline affinity, as indicated by high Nb/Y ratios (0.88 - 1.82). Compared to MORB-type basalts, they are enriched in FeO_t (11.73-14.70 wt%), TiO_2 (1.84-2.85 wt%), and P_2O_5 (0.16-0.56 wt%). They are also markedly enriched in Zr (148-324 ppm), Nb (21.3-65.2 ppm), Ta (1.69-5.40 ppm), and Th (2.45-9.80 ppm). N-MORB-normalized incompatible element patterns show strong enrichment of LILE relative to HFSE and regularly decreasing trends from Ba to Yb, closely resembling those of intra-oceanic alkaline basalts (OIB; Sun and McDonough, 1989) (Fig. 6g). Chondrite-normalized REE patterns are characterized by pronounced enrichment of LREE relative to both MREE and HREE (Fig. 6h), with high $(La/Sm)_N$ (2.26-3.33), $(Sm/Yb)_N$ (3.05-6.63), and $(La/Yb)_N$ (7.01-20.08) ratios typical of ocean island basalts. In tectonic discrimination diagrams, these rocks plot within the OIB field, indicating a subduction-unrelated within-plate setting (Fig. 6i; Saccani, 2015).

Petrogenetic and tectonic implications

Petrological, geochemical, and lithostratigraphic evidence indicates that the Bajgan Complex represents meta-ophiolitic successions formed in oceanic tectonic settings characterized by different mantle source compositions. N-MORB protoliths were generated at mid-ocean ridges from depleted mantle sources, whereas E-MORB protoliths reflect variable degrees of plume-related enrichment superimposed on a MORB mantle source. In contrast, the strongly enriched alkaline basalts were generated in within-plate oceanic seamount environments associated with plume-type mantle upwelling. These data collectively suggest spatial and temporal variations in mantle source enrichment and melting conditions during the formation of the oceanic lithosphere now preserved in the Bajgan Complex.

SUBDUCTION-RELATED OPHIOLITES IN THE NORTH MAKRAN DOMAIN: THE TECTONO-STRATIGRAPHIC ARCHITECTURE

The subduction-related ophiolites include two tectono-stratigraphic units, namely the Ganj Complex and the Sorkhband Ophiolites, showing different structural positions and stratigraphic architectures (Figs. 2, 7). In fact, the Ganj Complex is the uppermost tectonic unit in the structural stack of the North Makran domain whereas the Sorkhband Ophiolites are the lowermost coherent ophiolite (Fig. 7b). These subduction-related ophiolites are separated from each other by the Band-e-Zeyarat Ophiolites, the Durkan Complex, and the Bajgan Complex, representing the subduction-unrelated ophiolites of the North Makran domain.

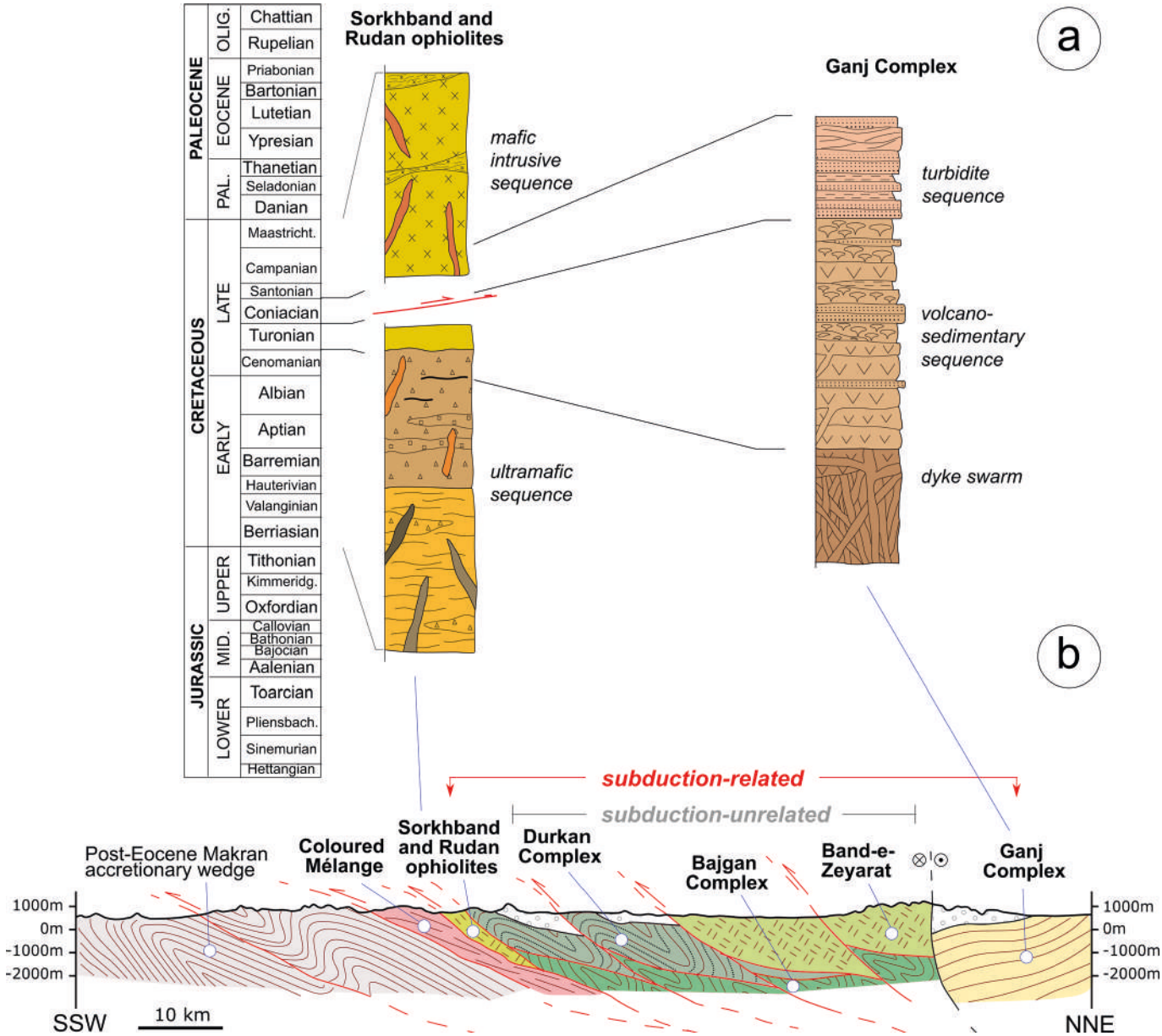

Fig. 7 - a) Lithostratigraphic columns of the subduction-related tectonic units of the North Makran Domain and b) simplified geological cross-section (see Fig. 2 for its location).

The Ganj Complex

The Ganj Complex represents a non-metamorphic Turonian-Cenomanian volcanic arc. The stratigraphic succession is >2000 m thick and composed of a basal dyke swarm, a volcano-sedimentary sequence, and a turbidite succession (Figs. 7a, 8a-c; Barbero et al., 2020a; Hajimohammadi et al., 2025; GholamiZadeh et al., 2025a). Based on Dilek and Furnes (2011), the stratigraphic architecture of this complex and the affinity of its magmatic rocks (Barbero et al., 2020a) allow us to classify the Ganj Complex as volcanic arc type ophiolite. The age constraints on this Complex consists of nannoplankton ages of the marls within the upper part of the volcano-sedimentary sequence and the turbidite succession (see Barbero et al., 2020a and details therein). The dyke swarm includes subparallel to cross-cutting andesitic, dacitic, rhyolitic, and subordinate basaltic dykes (Fig. 8a). Sills at its top mark the transition to the volcano-sedimentary sequence. The volcano-sedimentary succession includes alternating massive lava flows, pillow lavas, lava breccia, and minor sedimentary rocks. The massive flows dominate the lower part, while pillow lavas (Fig. 8b) and thin turbidite beds increase upward (Fig. 8c; Shaker Ardakani et al., 2009). Soft clasts of silty marl and marly limestone occur between pillow lavas. Textural and structural features, together with columnar basalts, point to subaerial to very shallow-water emplacement (Barbero et al., 2020a; Hajimohammadi et al., 2025). The turbidite unit consists of medium- to thin-bedded arenite passing upward into laminated silty marl and marly limestone. The arenite contains volcanic and carbonate fragments, along with shell and gastropod remains, indicating mixed sediment input from coeval volcanic arc and carbonate platform sources. Deposition occurred in an outer platform setting influenced by a river delta within a relatively shallow marine environment in an extensional intra-arc setting (Barbero et al., 2020a).

Structurally, this complex constitutes a 38 km-long and 15 km-wide arc-shaped tectonic unit sandwiched between the Jaz Murian depression and the subduction-unrelated Band-e-Zeyarat Ophiolites. Unfortunately, the basement of the volcanic arc succession is not exposed, as it probably lies beneath the Jaz Murian depression. The tectonic contact with the Band-e-Zeyarat Ophiolites corresponds to a thrust zone, although the steep N-S to NW-SE Jiroft Fault reworks the low-angle thrusts. Eocene sedimentary units rest unconformably on top (Barbero et al., 2020a). The Ganj Complex records two main deformational stages (Barbero et al., 2020a). The first phase produced gentle, upright folds with N-S to NW-SE-trending fold axes and a disjunctive axial-planar cleavage. The subsequent brittle phase generated high-angle strike-slip and normal faults that fragmented the complex into several tectonic slices. Both the Ganj Complex and the overlying Eocene deposits lack orogenic metamorphism, indicating deformation at shallow structural level.

The Sorkhband Ophiolites

The Sorkhband Ophiolites include two tectonic slices (Fig. 7a; Rajabzadeh and Moosavinasab, 2013; Delavari et al., 2016). The upper slice is composed of a ~100 m-thick sequence of coarse-grained gabbro intruded by fine-grained gabbro dykes. The lower slice consists predominantly of upper mantle peridotites with remnants of lower oceanic crust at the top. The base of this slice shows layered diopside-bearing harzburgites including minor dunite lenses and olivine clinopyroxenite to olivine websterite dykes. Up-section, harzburgite grades into thick dunite containing wehrlite and websterite bands, also intruded by olivine-bearing clinopyroxenites (Fig. 8d). Chromitites occur as disseminated to massive ore bodies within the dunite and as bands within mantle peridotite (Fig. 8e; Moghadam et al., 2022). The stratigraphic features of the Sorkhband ultramafic rocks indicate that they represent a mantle-lower crust transition formed within a forearc setting (Moghadam et al., 2022; Barbero et al., 2025). Based on Dilek and Furnes (2011), the lower unit of the Sorkhband ophiolite can be classified as SSZ-type ophiolite. No radiometric ages are available in literature for these ophiolites. However, according to their structural position between Jurassic and Cretaceous ophiolites and meta-ophiolites some authors have suggested a Cretaceous age (Ghazi et al., 2004; Delavari et al., 2016).

The structural setting of the Sorkhband Ophiolites is dominated by the localization of the deformation along their basal and roof tectonic contacts, which are characterized by NW-SE striking and NE-dipping thrust zones separating the Sorkhband Ophiolites from the Coloured Mélange and the Bajgan Complex, respectively (Figs. 2, 7b). The basal contact consists of a several-hundred-metre-thick shear zone containing boudinaged marbles, meta-basalts and serpentinized peridotites aligned along gently NE-dipping NW-SE shear planes, with S-C fabrics indicating top-to-the-SW shearing. The roof contact displays similar shear-zone characteristics and includes slices of amphibolites from the Bajgan Complex; meso-scale indicators show top-to-the-SW to top-to-the-S shearing (Fig. 8f).

SUBDUCTION-RELATED OPHIOLITES IN THE NORTH MAKRAN DOMAIN: GEOCHEMICAL AND PETROGENETIC FEATURES

This section summarizes the geochemical features and petrogenetic constraints of the Ganj Complex magmatic rocks as documented by Barbero et al. (2020b). The volcanic and subvolcanic rocks of the Ganj Complex include a wide spectrum of compositions ranging from basalt and basaltic andesite to andesite, dacite, and rhyolite. These lithologies occur as dykes, massive lava flows, and pillow lavas, and collectively define compositionally diverse but genetically related magmatic suites. All samples display a clear sub-alkaline affinity, as indicated by consistently low Nb/Y ratios (0.06-0.33), low contents of compatible elements (e.g., Cr, Ni, Co), enrichment of Th relative to Nb, and systematic enrichment of LREE relative to HREE. Based on immobile trace element systematics and REE distributions, the volcanic and subvolcanic rocks can be grouped into three main geochemical associations corresponding to calc-alkaline (CA), island arc tholeiitic (IAT), and volcanic arc rocks with a marked adakitic signature (ADK).

Calc-alkaline rocks

Calc-alkaline rocks comprise both dykes and massive lava flows and are dominated by dacites and rhyolites, with subordinate basaltic andesites and andesites. They exhibit wide compositional variability, with SiO_2 contents ranging from 56.8 to 74.3 wt% and Mg# values spanning from primitive to highly evolved compositions (Mg# = 67 - 8). TiO_2 (0.24 - 1.59 wt%), P_2O_5 (0.02 - 0.45 wt%), Zr (76 - 236 ppm), and Y (15 - 49 ppm) are generally low and decrease with increasing differentiation, whereas compatible element abundances are very low, reflecting advanced fractional crystallization (e.g., Cr <53 ppm; Ni <18 ppm). Major and trace element covariation trends indicate a calc-alkaline evolutionary path dominated by fractionation of clinopyroxene, hornblende, and magnetite relative to plagioclase, as shown by decreasing TiO_2 and FeO_t and increasing Y/Sc ratios with increasing differentiation (Barbero et al., 2020b). N-MORB-normalized incompatible element patterns display strong enrichment in Th, U, La, and Ce coupled with pronounced negative Ta, Nb, P, and Ti anomalies, a hallmark of calc-alkaline arc magmatism (Fig. 9a). Chondrite-normalized REE patterns further support a calc-alkaline affinity, as testified by marked LREE/HREE and MREE/HREE enrichment (Fig. 9b). Based on REE contents, Barbero et al. (2020b) identified two subgroups independent of the degree of differentiation, the REE patterns of which are interpreted to reflect variable mantle source enrichment. One subgroup shows steeply fractionated REE patterns with strong LREE and MREE enrichment relative to HREE (La_N/Yb_N = 3.3 - 5.5; Sm_N/Yb_N = 1.9 - 2.3), whereas the other displays more modest LREE enrichment and nearly flat MREE-HREE patterns (La_N/Yb_N = 1.7 - 2.3; Sm_N/Yb_N = 1.1 - 1.6). Th enrichment is particularly pronounced (9 - 30 times N-MORB values) and, together with the overall geochemical signature, is consistent with a calc-alkaline affinity (e.g., Pearce, 1983). This interpretation is confirmed by the discrimination diagram in Fig. 9c.

Island arc tholeiites (IAT)

IATs consist of basalts, basaltic andesites, and andesites occurring as dykes, massive lavas, and pillow lavas. These rocks show a clear tholeiitic affinity, as indicated by systematic increases in TiO_2 and FeO_t from basalts to basaltic andesites, followed by decreases in the most evolved compositions. At comparable differentiation levels, they contain higher TiO_2 (0.53 - 2.02 wt%), Cr (12 - 336 ppm), and Co (19 - 40 ppm)

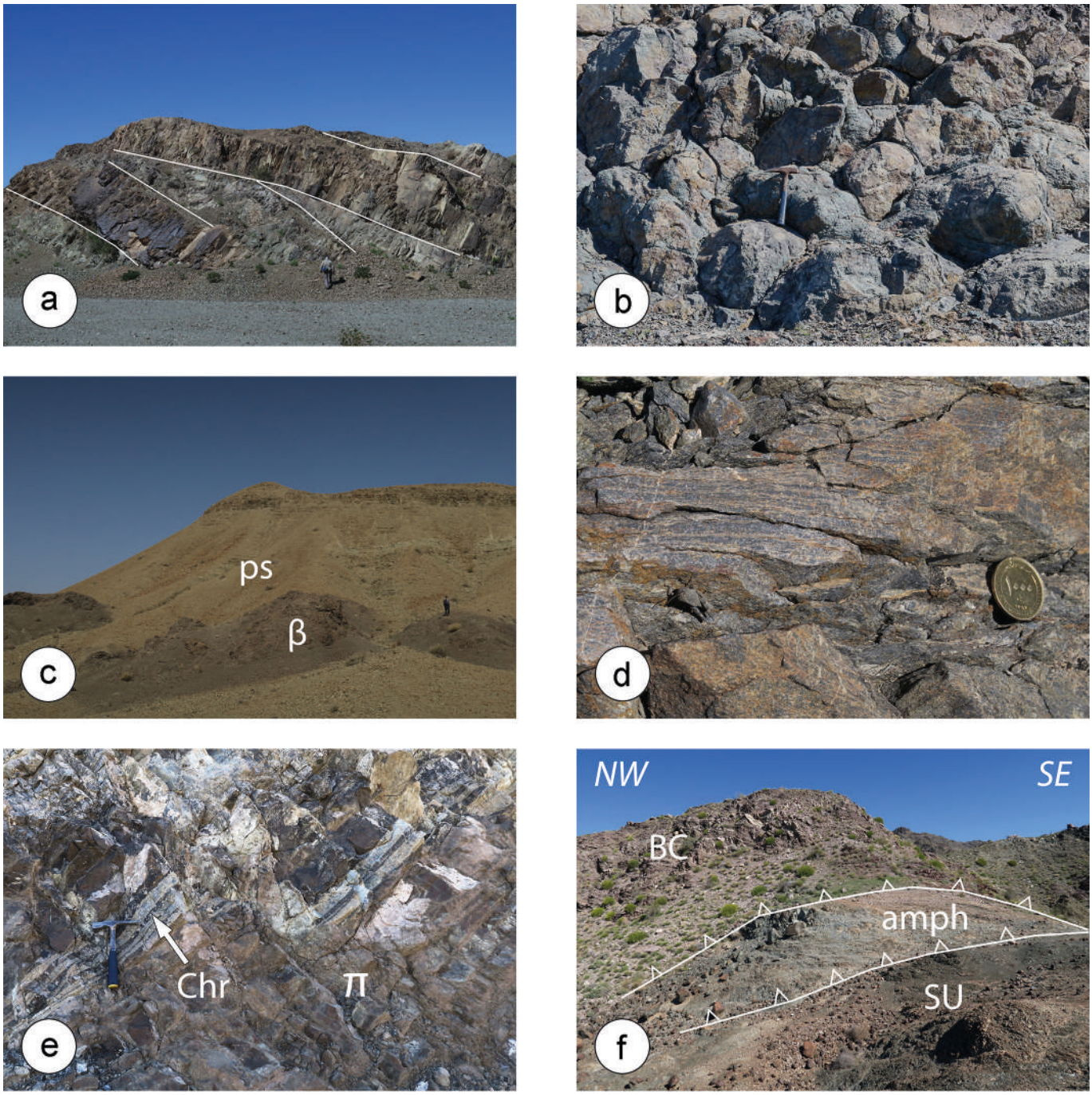

Fig. 8 - Field occurrence of the subduction-related ophiolites from the Ganj and Sorkhband units. Ganj Complex: a) dyke swarm including sub-parallel to crosscutting andesitic, dacitic, rhyolitic, and subordinate basaltic dykes. White lines indicate dyke boundaries; b) pillow lava flows from the volcanic sequence; c) relationships between pillow lavas (β) and pelagic sedimentary rocks (ps). Sorkhband Ophiolites: d) olivine-bearing clinopyroxenite; e) bands of chromitite (Chr) in mantle peridotite (π); (f) Sorkhband unit (SU) roof tectonic contact with the Bajgan Complex (BC) displaying shear-zone characteristics; meso-scale indicators show top-to-the-SW shearing. The sheared tectonic contact includes slices of amphibolites from the Bajgan Complex (amph).

and lower Y (9.5 - 32.9 ppm) than CA rocks. Their N-MORB-normalized incompatible element patterns are characterized by pronounced negative Nb and Ta anomalies, relative enrichment in Th and Ba, and the absence of Ti and P negative anomalies (Fig. 9a). Chondrite-normalized REE patterns show slight LREE enrichment relative to HREE, nearly flat MREE-HREE patterns (Sm_N/Yb_N = 1.2 - 1.8), and weak or absent Eu anomalies (Fig. 9b). Overall trace element characteristics closely resemble those of island arc tholeiites (e.g., Pearce, 1983;) as summarized in the discrimination diagram in Fig. 9c.

Volcanic arc rocks with adakitic signature

These volcanics comprise basaltic to basaltic andesitic pillow lavas and massive flows characterized by relatively primitive compositions (Mg# = 65 - 71) and limited fractional crystallization. These rocks are characterized by relatively low TiO_2 (0.53 - 0.94 wt%) and very low Y contents (7.64 - 11.2 ppm), as well as low contents of compatible elements (Cr = 62 - 144 ppm; Co = 20 - 25 ppm; Ni <31 ppm). A distinctive feature is their exceptionally high Sr contents (380 - 982

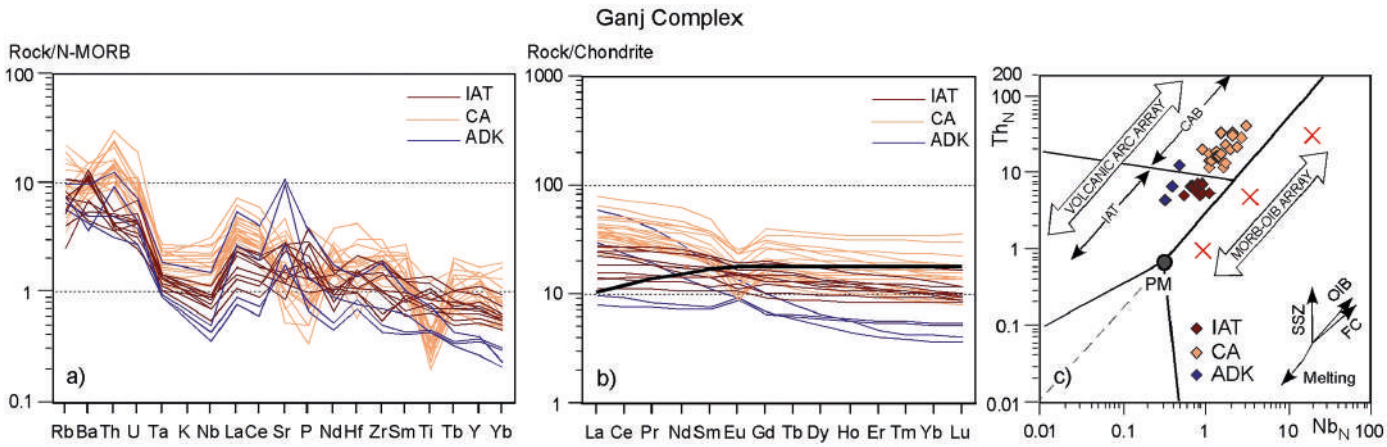

Fig. 9 - N-MORB normalized incompatible element patterns (a), Chondrite-normalized REE patterns (b), and N-MORB normalized Th vs. Nb discrimination diagram of Saccani (2015) (c) for subvolcanic, volcanic, and metavolcanic rocks from the subduction-related ophiolites from the North Makran domain. Normalizing values are from Sun and McDonough (1989). Red crosses in c) indicate the composition of normal (N-MORB) and enriched (E-MORB) mid-ocean ridge basalts, as well as alkaline ocean island basalt (OIB). Data from Sun and McDonough (1989). Vectors in c) indicate the trends of compositional variations due to the main petrogenetic processes (OIB: ocean island-type - plume-type - component enrichment; FC: fractional crystallization; SSZ: supra-subduction zone component enrichment). Arrows in c) broadly indicate the compositional variation of island arc tholeiites (IAT) and calc-alkaline basalts (CAB); data from Saccani (2015). Other abbreviations, CA: calc-alkaline rocks, ADK: volcanic arc rocks with adakitic signature.

ppm). These geochemical features clearly set them apart from CA and IAT rocks. N-MORB-normalized incompatible element patterns show strong enrichment in Th and Sr relative to Nb and Ta and very low HFSE contents from Hf to Yb (Fig. 9a). Chondrite-normalized REE patterns display extremely low HREE abundances (Yb_N = 4 - 6) and define two subgroups: one with steeply fractionated REE patterns and very high $(La/Yb)_N$ (8 - 14) and $(Sm/Yb)_N$ (3 - 4), and another with gently sloping REE patterns and much lower fractionation ratios (La_N/Yb_N ~1.6; Sm_N/Yb_N ~1.4, Fig. 9b). In tectonic discrimination diagrams, the strongly fractionated subgroup plots within the calc-alkaline field, whereas the less fractionated subgroup overlaps with the IAT field (Fig. 9c). Although these rocks do not fully satisfy the compositional criteria of either high-silica or low-silica adakites (e.g., Castillo, 2006; Richards and Kerrich, 2007), their Sr-Y-Yb systematics indicate a pronounced adakitic geochemical signature.

Petrogenetic implications

Petrogenetic modelling based on Cr-Y and Ba/Th - Th/Nb co-variation, as well as REE compositions (Barbero et al., 2020a) indicates that calc-alkaline rocks formed by ~10-12% partial melting of a depleted spinel-facies lherzolite mantle previously affected by MORB extraction and subsequently metasomatized by subduction components, including ~0.5-0.7% sediment-derived melt addition. Island arc tholeiites resulted from higher degrees of partial melting (~15-17%) of a similarly depleted mantle source predominantly modified by subduction-derived aqueous fluids, with a minor sediment-derived melt contribution.

The adakitic-signature rocks can be explained by ~15% partial melting of a depleted mantle source metasomatized by variable amounts (~1-3%) of an adakitic melt component. Collectively, these data indicate that the volcanic and subvolcanic rocks of the Ganj Complex formed in a volcanic arc tectonic setting along the southern margin of the Lut Block during the Late Cretaceous, recording variable mantle source metasomatism, melting conditions, and magma evolution within a single arc system.

DISCUSSION

Mode and tempo for subduction-unrelated and subduction-related ophiolites in the North Makran domain

The systematic analysis and integration of the stratigraphic, structural, petrological, and age data from the ophiolites of the North Makran domain allow us to evaluate the mode and tempo of the oceanic lithosphere accretion and evolution with time in the Makran sector of the Neo-Tethys. Using this approach, we identified three main stages of oceanic lithosphere formation from Late Jurassic to Late Cretaceous. Fig. 10 shows the comparison with the age of the magmatic events and their geochemistry, according to three geochemical proxies. The Th_N-Nb_N proxy (Fig. 10a) indicates enrichment in subduction-related chemical components during magma genesis, discriminating thus between subduction-related and subduction-unrelated ophiolites (e.g., Pearce, 2008; Saccani, 2015). The Zr-Y and Nb-Zr proxies (Figs. 10b, c) represent key petrogenetic indicators for OIB-type chemical components during magma genesis (e.g., LeRoex et al., 1983; Fitton et al., 2003), allowing us to discriminate between MOR-type and Plume-Type ophiolites (*sensu* Dilek and Furnes, 2011).

The first stage of oceanic formation lasted from the Late Jurassic (or earlier) to the Early Cretaceous, when the protoliths of the HP-LT meta-ophiolites of the Bajgan Complex and the Band-e-Zeyarat Ophiolites were formed (Fig. 10). Their reconstructed similar magmatic stratigraphy with the occurrence of hundreds to 2 km-thick gabbros and sheeted dykes is well comparable with MOR-type ophiolites of Dilek and Furnes (2011). Accordingly, the pelagic nature of the sedimentary and meta-sedimentary rocks associated with basalt and meta-basalt of the Band-e-Zeyarat Ophiolites and the Bajgan Complex, respectively, indicate a deep-water basin (Pandolfi et al., 2021; Barbero et al., 2023c), which is the typical geodynamic setting where mid-ocean ridge develops. Consistently, the geochemical signature of the magmatic rocks from the Bajgan Complex and the Band-e-Zeyarat Ophiolites range from N- to E-MORB (Pandolfi et al., 2021;

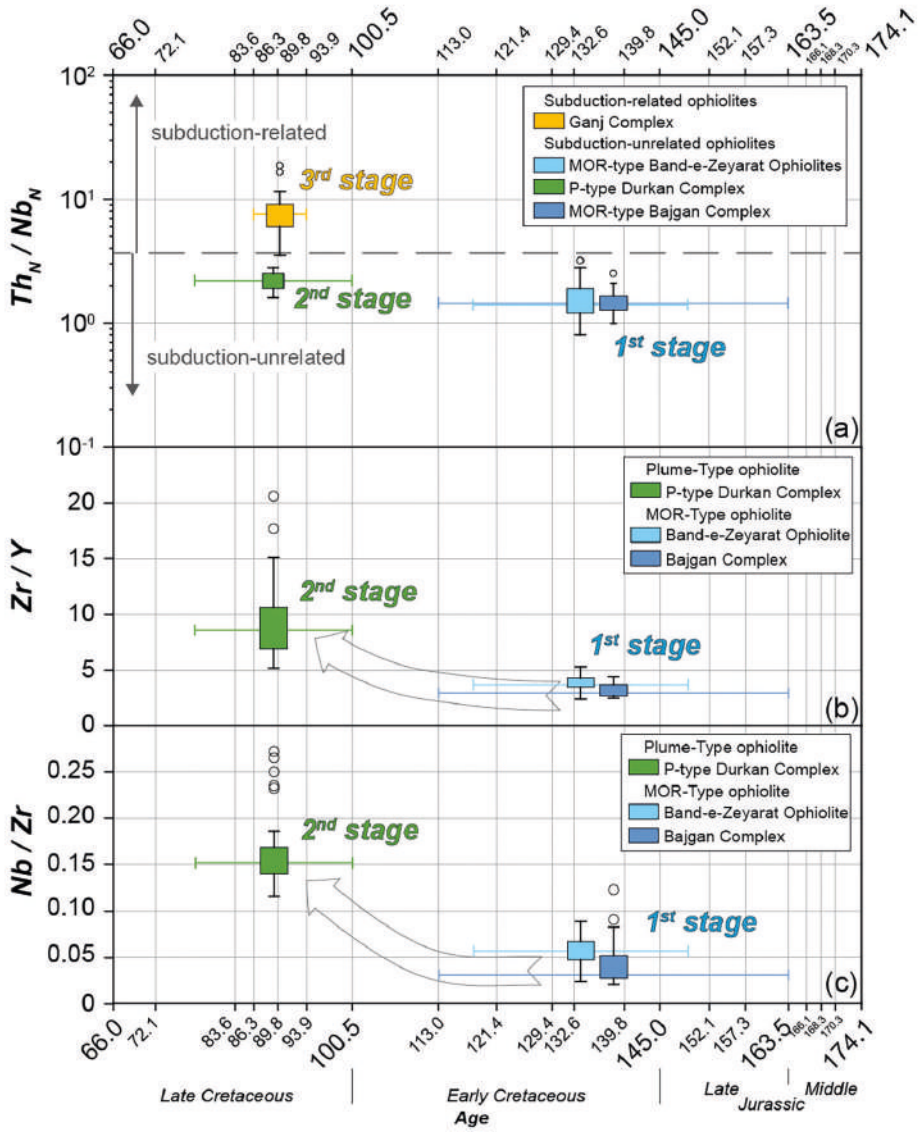

Fig. 10 - Evolution of age and geochemistry of the magmatic stages recognized in the ophiolites of the North Makran domain. The panel (a) shows the time variation of the Th_N-Nb_N geochemical proxy, which indicates the contribution of subduction-related chemical components during the ophiolite genesis (Pearce, 2008; Saccani, 2015). Black dashed line represents the Th_N-Nb_N ratios distinguishing value for subduction-related and subduction-unrelated ophiolites calculated from the discrimination diagram of Saccani (2015); Panels (b) and (c) show the time variations of the Zr-Y and Nb-Zr proxies, which indicate the contribution of Ocean Island Basalt (OIB) chemical component during the genesis of subduction-unrelated ophiolites. The arrow indicates the time-dependent increase in OIB-type chemical components in the ophiolites of the North Makran domain. Data sources: Barbero et al. (2020a, 2020b, 2021b, 2023c; Pandolfi et al., 2021; Saccani et al., 2024).

Barbero et al., 2020b, 2023c) with relatively low Th_N/Nb_N ratios, indicating the formation of the oceanic lithosphere during this stage within a subduction-unrelated MOR setting (Fig. 10a).

The second stage of oceanic formation occurred during the Late Cretaceous and is characterized by a remarkable change in the nature and petrogenetic processes of the North Makran oceanic lithosphere. In fact, the stratigraphy and the geochemistry of the volcanic rocks of the Durkan Complex testifies for OIB-influenced magmatism (P-MORB and alkaline rocks; Fig. 10) in various depositional environments. These include deep-water pelagic, deep-water slope, and shallow-water carbonate platform environments. Based on stratigraphic and petrological constraints, Barbero et al. (2021a, b) interpreted the Durkan Complex as a seamount chain associated with a within-plate and plume-related magmatism (P-Type ophiolite *sensu* Dilek and Furnes, 2011). The analysis of geochemical proxies shown in Figs. 10 (b,c) allows us to prove a temporal variation on the contribution of OIB-type components for the magma genesis and mantle sources evolution. In fact, magmatic rocks of the Durkan Complex formed during the second stage show Zr/Y and Nb/Zr ratios significantly higher than first stage rocks, indicating that in the Late Cretaceous the North Makran Ocean was largely characterized by a significant influence from plume-type components. This highlights a compositional variation of the subduction-unrelated ophiolites of the North Makran from the Early Cretaceous to the Late Cretaceous, suggesting the time-dependent increase of contribution of a mantle plume and/or mantle plume chemical components during the magma genesis and mantle source evolution (Figs. 10b, c).

The time-dependent evolution from the first stage to the second stage of oceanic crust formation is well shown in Fig. 11. Fitton et al. (1997, 2003) have shown that a logarithmic Nb/Y versus Zr/Y diagram is an effective tool for distinguishing plume-influenced basalts from non-plume basalts. Icelandic basalts (plume-related) and N-MORB (non-plume) define two distinct, subparallel linear arrays in this space. Using the lower boundary of the Icelandic array as a reference, Fitton et al. (1997) introduced the parameter ΔNb, which quantifies Nb excess or depletion, where plume-related basalts have $\Delta Nb > 0$, whereas non-plume MORB have $\Delta Nb < 0$. Variations along each array mainly reflect different degrees of partial melting, with lower degrees of melting producing higher Zr/Y and Nb/Y ratios. However, simple melting models show that ΔNb is largely insensi-

tive to melting degree and therefore reflects mantle source characteristics rather than melting processes. Fig. 11 shows that the Early Cretaceous N-MORB and some of the Early Cretaceous E-MORB have negative ΔNb indicating no, or negligible, plume-influence. In contrast, part of the Early Cretaceous E-MORB and Late Cretaceous P-MORB and alkaline basalts have positive ΔNb, which indicates a marked plume-influence for these rocks. Fig. 11 also shows that the best fit line calculated for all rock samples is very similar to the mixing line between the N-MORB and OIB compositions of Sun and McDonough (1989), suggesting that the petrogenesis of most of the North Makran ophiolites is consistent with various extent of plume-ridge interaction. These observations suggest that the North Makran Ocean was weakly affected by plume activity during the Late Jurassic-Early Cretaceous and indicate a progressive increase influence of plume activity on the oceanic crust formation, reaching a peak in the Late Cretaceous.

Based on stratigraphic and petrological constraints from the Complex, the third stage of oceanic accretion was marked by the formation of the Late Cretaceous Ganj volcanic arc at the northern margin of the oceanic basin, which testifies for subduction activity (Barbero et al., 2020a; Barbero et al., 2025). In fact, the volcanic facies, the composition of the volcaniclastic arenites, and the shallow-water outer platform depositional environment of the Ganj Complex succession (Barbero et al., 2020a; Hajimohammadi et al., 2025; GholamiZadeh et al., 2025a) indicate crust formation within a subduction-related volcanic arc setting (*sensu* Dilek and Furnes, 2011; Fig. 10a). Accordingly, the petrogenesis of the magmatic rocks of the Ganj Complex is strongly controlled by the input of slab-released chemical components to the asthenospheric mantle wedge above the subducting slabs. This process is well exemplified by the Th_N/Nb_N ratios, which are significantly higher in the Ganj rocks with respect to those of the subduction-unrelated ophiolites (Fig. 10a) and are greater than the Th_N/Nb_N ratios of the volcanic arc array of Saccani (2015). Thus, during the Late Cretaceous the available data indicate the contemporaneous formation of crustal rocks within a subduction-unrelated oceanic setting dominated by common plume activity and subduction-related setting providing a key constraint for the geodynamic significance of the ophiolites of the North Makran domain.

The origin of the ophiolites of the North Makran domain in the geodynamic evolution of the Neo-Tethys

The multidisciplinary data from the ophiolites of the North Makran domain are here discussed to propose a new reconstruction of oceanic lithosphere accretion in the Makran sector of the Neo-Tethys from the Jurassic to the Late Cretaceous. Below, we discuss the variations of the tectonic setting of formation of the oceanic lithosphere in response to geodynamic processes such as oceanic spreading, subduction initiation and evolution, and mantle plume activity. To this end, we follow the general tectonic framework for the convergent and accretionary stages as proposed by Burg (2018) and Barbero et al. (2025).

Late Jurassic-Early Cretaceous: Oceanic lithosphere accretion in mid-ocean ridge and forearc settings

During this phase, the oceanic lithosphere formation within mid-ocean ridge setting is recorded by the tectono-stratigraphic and tectono-magmatic architecture of the HP-LT Bajgan Complex meta-ophiolites and the Band-e-Zeyarat Ophiolites. The evidence from the North Makran domain aligns with regional-scale paleogeographic reconstructions of the whole Neo-Tethys realm (Dercourt et al., 1986; Şengör et al., 1988; Robertson and Searle, 1990; Stampfli and Borel, 2002; Barrier et al., 2018). In fact, this ocean evolved between the Arabia-India and the Eurasia plates since the Late Permian with rifting along the northern Gondwana margin followed by spreading stage within a MOR setting as demonstrated by remnants of ophiolitic units strongly deformed

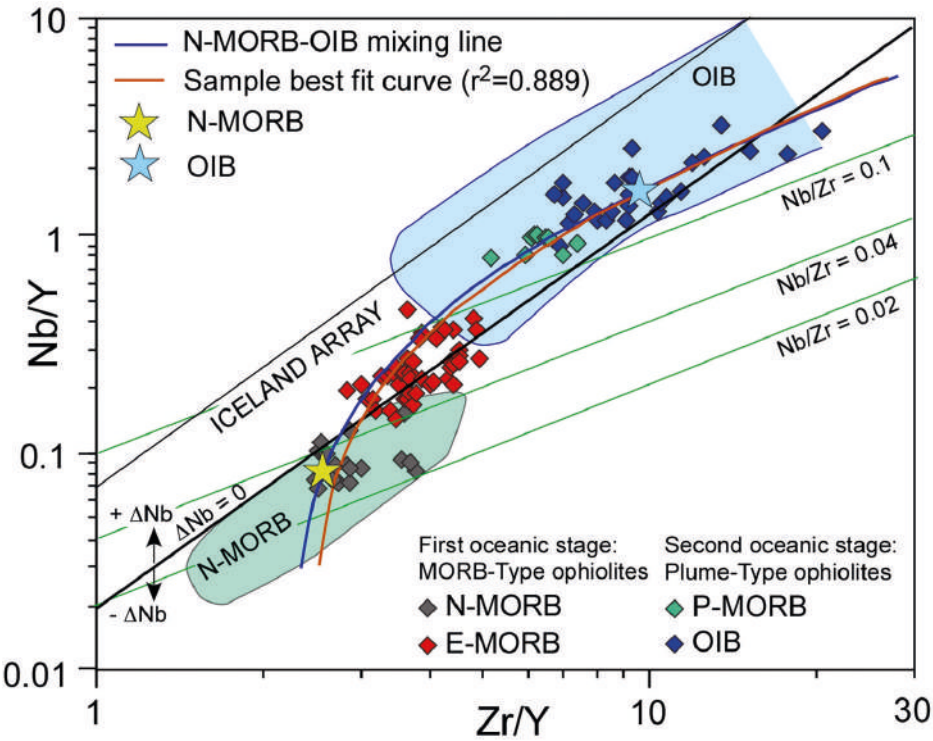

Fig. 11 - Nb/Y versus Zr/Y diagram (after Fitton et al., 2003) for subvolcanic, volcanic, and metavolcanic rocks from the subduction-unrelated ophiolites and meta-ophiolites from the North Makran domain. Iceland array and compositional fields for N-MORB and OIB are from Fitton et al. (2003, and references therein). Stars indicate the compositions of N-MORB and OIB of Sun and McDonough (1989). Abbreviations: MORB: mid-ocean ridge basalt; N-: normal-type; E-: enriched-type; P-: plume-type; OIB: alkaline ocean island basalt.

within the Oman Mountains and the Zagros collisional belts (Robertson and Searle, 1990; Chauvet et al., 2011; Ghasemi and Talbot, 2006; Moghadam et al., 2017). The formation of subduction-unrelated MOR-type oceanic lithosphere of the Bajgan Complex and the Band-e-Zeyarat ophiolites can likely be restored within this regional MOR of the Neo-Tethys (Fig. 12; see Barbero et al., 2025 and discussion therein). According to Dilek and Furnes (2011), the pluri kilometric thickness of the gabbros and sheeted dykes complexes of the Band-e-Zeyarat Ophiolites indicated that this MOR was likely characterized by medium to fast spreading rate.

In the Early Cretaceous, this geodynamic scenario changed due to the regional onset of shortening kinematics within the Neo-Tethys Ocean due to a change in relative motion of the major continental plates (e.g., Torsvik et al., 2012; Jagoutz et al., 2015; Gaina et al., 2015; Barrier et al., 2018). In fact, the convergence between Arabia-India and Eurasia plates started during the Early Cretaceous, causing the nucleation of subduction zones associated with HP/LT metamorphism and arc magmatism (Agard et al., 2006; Angiboust et al., 2016; Moghadam et al., 2017; Rolland et al., 2020). In the North Makran domain, the stratigraphic and geochemical features of the Sorkhband ultramafic rocks indicate its formation within a forearc setting (e.g., Delavari et al., 2016; Moghadam et al., 2022), likely testifying to nucleation of an intra-oceanic subduction zone within the Makran sector of the Neo-Tethys due to this regional-scale geodynamics (Fig. 12). In the Makran, there are no remnants of coherent and complete ophiolite preserving the oceanic crust formed within a deep-water forearc during this period. However, Early Cretaceous volcanic arc rocks associated with pelagic sedimentary rocks are found within the Coloured Mélange and interpreted as remnants of Early Cretaceous forearc oceanic crust that were tectonically disrupted and deformed within the accretionary prism during the late Paleocene - Eocene (Saccani et al., 2018; Barbero et al., 2025).

The main consequence of the nucleation of this intra-oceanic subduction is the identification of two oceanic branches within the Neo-Tethys realm in the Early Cretaceous (e.g., Rolland et al., 2020; Barbero et al., 2025). In the Makran, Barbero et al. (2025) proposed that the ophiolites of the North Makran domain derived from the northern branch, named the North Makran Ocean, whereas fragments of the southern branch, named the Neo-Tethys, are now represented by part of the Coloured Mélange.

The Early Cretaceous geodynamic was characterized by the contemporaneous oceanic lithosphere accretion in both subduction-related and subduction-unrelated setting. In this period, in the North Makran Ocean the MOR was still active and producing subduction-unrelated type oceanic lithosphere as indicated by the age of the Bajgan Complex and the Band-e-Zeyarat Ophiolites (Fig. 12). Meanwhile, subduction-related oceanic lithosphere was forming above the forearc mantle wedge associated with the intra-oceanic subduction of the Neo-Tethys oceanic lithosphere (Fig. 12).

Late Cretaceous: Oceanic lithosphere accretion in volcanic arc and plume-related seamount settings.

This period was characterized by a significant change in the mode of oceanic lithosphere construction within the North Makran Ocean. No evidence of MOR-type ophiolites is recorded within the Late Cretaceous ophiolites of the North Makran domain, as N-MORBs of Late Cretaceous age have not so far been documented. On the contrary, the stratigraphy and geochemistry of the magmatic rocks from the Durkan and Ganj Complex testify to the onset of plume-related magmatism within the oceanic plate and arc-related magmatism at its border, respectively (Fig. 13). The stratigraphy of the Durkan Complex displays characteristics suggesting its formation within a seamount chain onto the Late Jurassic-Early Cretaceous MOR-type oceanic lithosphere (Fig. 13). The stratigraphic relationship between shallow-marine carbonate platform and volcanic rocks indicated that individual seamount of the chain reached ~ 4-5 km of elevation above the MOR-type oceanic crust.Accordingly, the P-MORB to alkaline affinities of the basalts and meta-basalts are indicative of

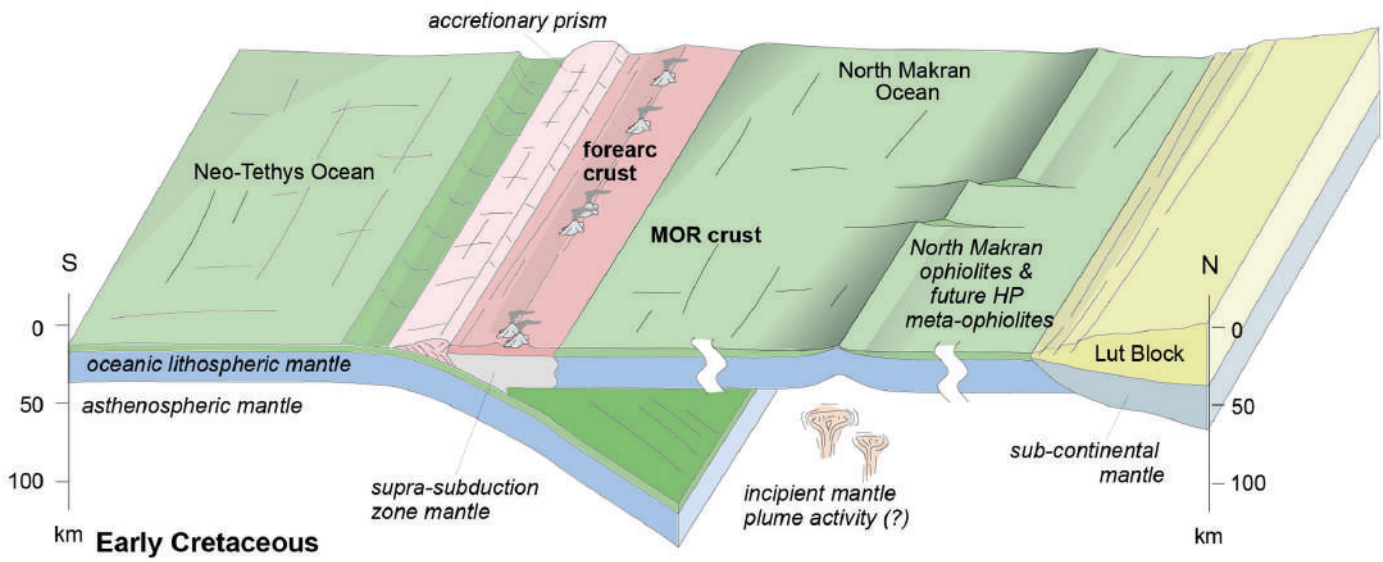

Fig. 12 - 3D sketch illustrating the geodynamic reconstruction of the North Makran Domain during the Early Cretaceous. In the southern part, convergence led to north-dipping subduction, resulting in the development of a southern accretionary prism. This prism was bounded to the north by a supra-subduction zone overlain by a forearc domain. In the northern sector, an extensional tectonic regime promoted ridge formation and the generation of mid-ocean ridge (MOR) crust progressively influenced by incipient mantle plume activity.

contribution from mantle plume activity during their formation, which is confirmed by petrogenetic modelling pointing to partial melting of OIB-type asthenospheric mantle within the garnet field during plume ascent (see Barbero et al., 2021b and discussion therein). Thus, the Durkan Complex is regarded as a subduction-unrelated P-type ophiolite (*sensu* Dilek and Furnes, 2011).

A completely different scenario can be depicted for the Ganj Complex. The stratigraphy, geochemistry of the magmatic rocks, and petrogenetic modelling indicate its formation within a volcanic arc setting above a subduction zone (Fig. 13). Barbero et al. (2025) proposed that the Ganj arc was associated with a newly established subduction zone, where the lithosphere of North Makran Ocean subducted beneath the Lut Block. In fact, the structural position at the top of the North Makran tectonic pile, relatively weak deformation, and shallow- to moderate-water depositional environments, as well as distinct geochemical features exclude the correlation of the Ganj Complex with the Early Cretaceous intra-oceanic arc. Kinematic reconstructions based on south-directed shear sense indicate that the Ganj arc originally formed north of the North Makran Ocean, along the Lut margin (Fig. 13; Barbero et al., 2025). According to arenite composition and provenance study, GholamiZadeh et al. (2025a) reached a similar conclusion, proposing the existence of two volcanic arcs associated with two distinct subduction zones. According to this evidence, the Ganj Complex represents a volcanic arc that was built onto the Late Jurassic-Early Cretaceous MOR-type oceanic lithosphere or on the thinned continental margin of the Lut Block. Unfortunately, the lack of exposure of the crustal basement of this arc or subsurface data does not allow the precise assessment of these two hypotheses. It is worth noting that while the subduction of the North Makran Ocean contributed to the formation of the Ganj arc, the intra-oceanic subduction of the Neo-Tethys was still active during the Late Cretaceous. This intra-oceanic subduction kept producing oceanic lithosphere in forearc domain, as testified by the IAT and calc-alkaline rocks found in the Coloured Mélange (Saccani et al., 2018; Barbero et al., 2025). In conclusion, the outstanding feature of the Late Cretaceous evolution of the North Makran Ocean was the construction of oceanic lithosphere within forearc and arc settings associated with two distinct subduction zones contemporaneously to the formation of subduction-unrelated oceanic lithosphere associated with a mantle plume.

Latest Cretaceous-Eocene: complete consumption of a composite oceanic lithosphere

During this phase, the composite subduction-related and -unrelated oceanic lithosphere of the North Makran Ocean was progressively closed to accommodate the regional-scale convergence kinematics between the Arabia and Eurasia plates (Agard et al., 2011; Barrier et al., 2018). According to Barbero et al. (2025), the consumption of this oceanic lithosphere was due to its northward subduction below the Lut Block. This subduction was associated with a subduction complex where fragments of the subducting lithosphere were incorporated via underplating at its base (Fig. 14). This process is testified by the deformation histories of the Band-e-Zeyarat Ophiolites, the Durkan Complex, and the Bajgan Complex, which record the latest Cretaceous - late Paleocene accretion of the oceanic lithosphere at different structural levels, from few kilometres (e.g., Band-e-Zeyarat and part of the Durkan Complex; Barbero et al., 2021a, 2023c) to 20-40 km (e.g., the Durkan and Bajgan Complexes, Pandolfi et al., 2021; Barbero et al., 2023b). It is worth noting that the oceanic lithosphere accreted by underplating processes corresponds to those formed within subduction-unrelated MOR- and P-Type settings in the earlier stages. This proposed scenario is supported by the tectono-metamorphic evolution of meta-ophiolites from the neighbouring collisional

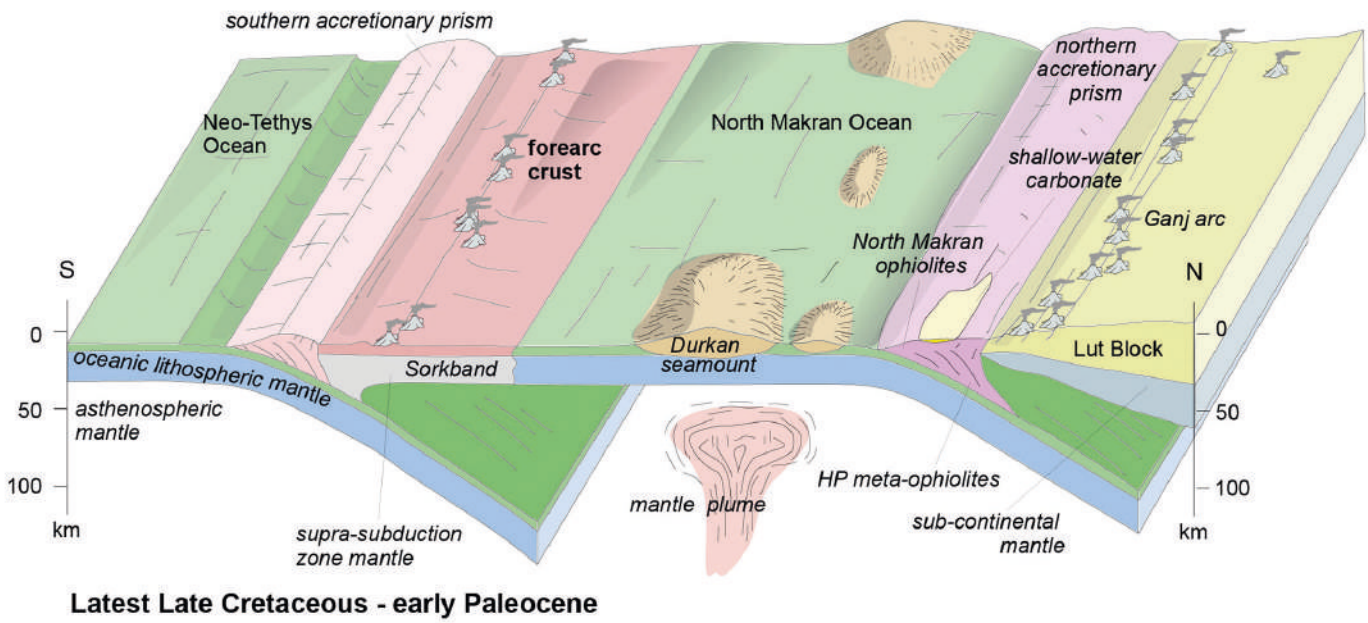

Fig. 13 - 3D Sketch illustrating the geodynamic reconstruction of the North Makran Domain during the latest Late Cretaceous to early Paleocene. The transition from extension to compression gave rise to a younger, north-dipping subduction zone in the North Makran Ocean. This produced a new accretionary prism where slices of mid-ocean ridge (MOR) crust were accreted at depth and deformed under high-pressure, low-temperature (HP-LT) metamorphic conditions. Shallow-marine carbonate platforms developed at the top of the prism. The Ganj volcanic arc developed northward as a result of this new subduction. Mantle plume activity in the region generated seamounts (e.g., Durkan) in the lower plate adjacent to the trench.

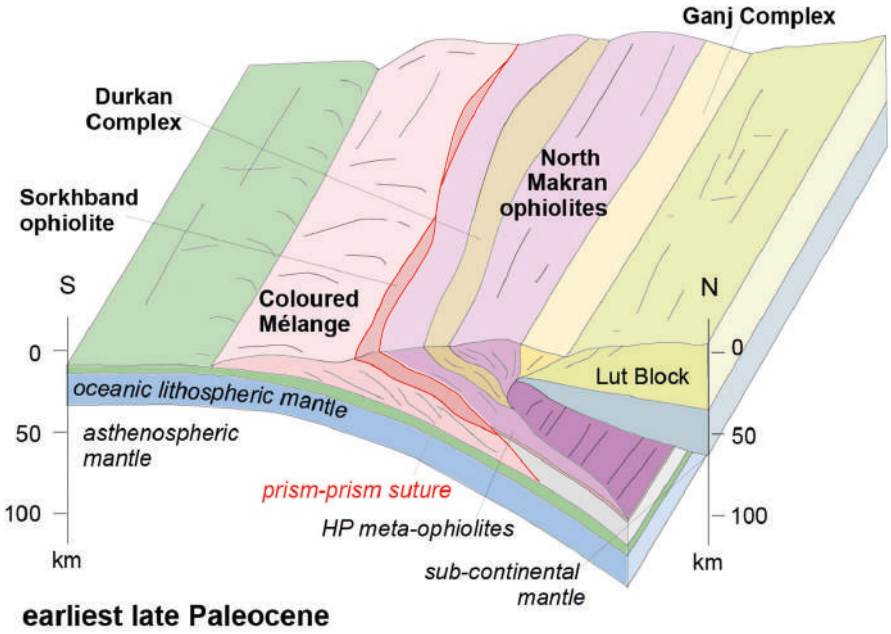

Fig. 14 - 3D sketch illustrating the geodynamic reconstruction of the North Makran Domain during the earliest late Paleocene (i.e., prior to the deposition of the late Paleocene - early Eocene sedimentary succession). The complete subduction of the North Makran Ocean resulted in the southern prism being thrust under the northern prism. This is represented today by the northernmost units of the North Makran domain. Along the suture zone between the two prisms, remnants of the supra-subduction zone (i.e., Sorkhband) were preserved. Evidence of mantle plume activity is instead represented by the Durkan Complex, which is embedded in the HP meta-ophiolites. The Coloured Mélange gradually formed at the front of the stack of units from the North Makran domain.

belts, which record HP-LT Late Cretaceous metamorphism achieved within a subduction complex along the southern margin of the Eurasia Plates (Agard et al., 2005; Angiboust et al., 2016; Omrani et al., 2017; Bröcker et al., 2021; Muñoz-Montecinos et al., 2021).

A key aspect of the deformative evolution of the North Makran domain is the evidence of intense shortening within the Band-e-Zeyarat Ophiolites, and the Durkan and Bajgan Complexes. In particular, the reverse shear zones characterizing these ophiolites indicate strong tectonic imbrication due to compressional tectonics. A similar structural architecture is observed in the subduction-related forearc oceanic lithosphere of the Sorkhband Ophiolites, demonstrating that the shortening ultimately propagates to the southern portion of the North Makran Ocean, within the former Cretaceous subduction-related forearc lithosphere (Fig. 14). The main effect of this compressive tectonic is the overthrust of the Sorkhband Ophiolites onto the Coloured Mélange, which, on the contrary, was built via offscraping and underplating within the Neo-Tethys subduction complex (Fig. 14; e.g., McCall and Kidd, 1982; Burg, 2018; Saccani et al., 2018; Barbero et al., 2025). Although deformation ages are not tightly constrained, the evidence that the youngest age of the blocks in the Coloured Mélange is early Paleocene (McCall, 1983), and upper Paleocene - Eocene deposits unconformably seal the major shear zones suggest a Paleocene age for this compressive phase (McCall, 1983; Barbero et al., 2023b, c). At larger scale, the forearc oceanic lithosphere of the Sorkhband Ophiolites marks the suture between the North Makran and the Neo-Tethys subduction complexes, which took place for the complete closure of the North Makran Ocean. Meanwhile, the southern Neo-Tethys Ocean was still opened and its subduction kept accommodating the convergence between Arabia-India and Eurasia Plates since the present day (Platt et al., 1985; Kopp et al., 2000; Regard et al., 2010; Burg, 2018).

CONCLUSION

The ophiolites of the North Makran domain (southeast of Iran) occur within a stack of tectonic units, which record the progressive incorporation of fragments of Neo-Tethys oceanic lithosphere within an accretionary complex during the convergence between the Arabian and Eurasian Plates. The integration of stratigraphic, structural, petrological, and geochemical data indicates the occurrence of both subduction-unrelated and subduction-related types of ophiolites (*sensu* Dilek and Furnes, 2011), documenting a long-lived and complex geodynamic evolution characterized by the interplay of different tectonic settings within the Makran sector of the Neo-Tethys during the Jurassic-Cretaceous times. Within this framework, the evolution of the North Makran oceanic lithosphere can be described as a multi-stage process. The oldest ophiolites so far documented in the North Makran domain record a Late Jurassic-Early Cretaceous formation of oceanic lithosphere mainly in a subduction-unrelated mid-ocean ridge setting, producing MOR-type ophiolites. Petrological constraints point to an increasing influence of plume-related components on magma genesis within this mid-ocean ridge during the Early Cretaceous. At the same time, the nucleation of an intraoceanic subduction system led to the development of forearc oceanic lithosphere and to the separation of the North Makran Ocean (to the north) from the main Neo-Tethys Ocean (to the south).

This early geodynamic configuration was followed in the Late Cretaceous, by a significant change in the mode of oceanic lithosphere formation marked by the coeval development of plume-related seamounts within the oceanic plate and volcanic arc magmatism along the northern margins of the North Makran Ocean, associated with subduction beneath the Lut Block. This stage documents the coexistence of subduction-unrelated and subduction-related oceanic lithosphere within the same basin, reflecting the interaction between mantle plume activity and multiple subduction zones. Continued convergence from the latest Cretaceous to the Eocene led to the progressive northward subduction of the North Makran Ocean beneath the Lut Block triggering accretion and deformation of its composite oceanic lithosphere and finally resulting in the complete closure of this basin and suturing of the North Makran and the Neo-Tethys subduction complexes.

Taken together, these results highlight the North Makran domain as a key natural laboratory for understanding how

oceanic lithosphere is generated, modified, and incorporated within convergent margins. More broadly, this review emphasizes that the evolution of the Neo-Tethys cannot be described by simple end-member models but instead reflect time-dependent and spatially variable interactions between mid-ocean ridge, mantle plume components, and multiple subduction zones. This study also points up that multidisciplinary studies integrating stratigraphic, structural, petrological, and chronological data remain essential for constraining processes governing the formation and consumption of ancient oceanic basins.

ACKNOWLEDGEMENTS

The research has been funded by the Darius Project (Head M. Marroni), PRA project of the Pisa University (Head S. Rocchi), and the IGG-CNR, FAR-2025 Project of the Ferrara University (Head E. Saccani). We sincerely thank Mr. Ahmad Behboodi for his assistance in organizing field work, and PhD student Ahmad Nateghpour from Kharazmi University for his help during field work. Rita Catanzariti, Marco Chiari, Federico Farina, Chiara Frassi, Antonio Langone, Valeria Luciani, Leila Vahedi, and Federica Zaccarini, are also thanked for the scientific contributions provided through the time.

REFERENCES

Agard P., Omrani L., Jolivet L. and Mouthereau F., 2005. Convergence history across Zagros (Iran): constraints from collisional and earlier deformation. Int. J. Earth. Sci., 94: 401-419. https://doi.org/10.1007/s00531-005-0481-4

Agard P., Monié P., Gerber W., Omrani J., Molinaro M., Meyer B., Labrousse L., Vrielynck B., Jolivet L. and Yamato P., 2006. Transient, syn-obduction exhumation of Zagros blueschists inferred from P-T, deformation, time, and kinematic constraints. J. Geoph. Res., 111 (B11). https://doi.org/10.1029/2005JB004103

Agard P., Omarani J., Jolivet L., Whitechurch H., Vrielynck B., Spakman W., Monié P., Meyer B. and Wortel R., 2011. Zagros orogeny: a subduction-dominated process. Geol. Mag., 148: 692-725. https://doi.org/10.1017/S001675681100046X

Allègre C.J. and Minster J.F., 1978. Quantitative models of trace element behaviour in magmatic processes. Earth Planet. Sci. Lett., 38: 1-25. https://doi.org/10.1016/0012-821X(78)90123-1

Angiboust S., Agard P., Glodny J., Omrani J. and Oncken O., 2016. Zagros blueschists: Episodic underplating and long-lived cooling of a subduction zone. Earth Planet. Sci. Lett., 443: 48-58. https://doi.org/10.1016/j.epsl.2016.03.017

Arvin M., Babaei A.A., Ghadami Gh., Dargahi S. and Shakerardekani A.R., 2005. The origin of the Kahnouj ophiolitic complex, SE of Iran: constraints from whole rock and mineral chemistry of the Bande-Zeyarat gabbroic complex. Ofioliti, 30: 1-14. https://doi.org/10.4454/ofioliti.v30i1.341

Balestro G., Festa A., Dilek Y. and Tartarotti P., 2015. Pre-Alpine extensional tectonics of a peridotite-localized oceanic core complex in the late Jurassic, high-pressure Monviso ophiolite (Western Alps). Episodes, 38 (4): 266-282. https://doi.org/10.18814/epiiugs/2015/v38i4/82421

Barbero E., Delavari M., Dolati A., Saccani E., Marroni M., Catanzariti R. and Pandolfi L., 2020a. The Ganj Complex reinterpreted as a Late Cretaceous volcanic arc: Implications for the geodynamic evolution of the North Makran domain (southeast Iran). J. Asian Earth Sci., 195: 104306. https://doi.org/10.1016/j.jseaes.2020.104306

Barbero E., Delavari M., Dolati A., Vahedi L., Langone A., Marroni M., Pandolfi L., Zaccarini F. and Saccani E., 2020b. Early Cretaceous Plume-Ridge Interaction Recorded in the Band-e-Zeyarat Ophiolite (North Makran, Iran): New Constraints from Petrological, Mineral Chemistry, and Geochronological Data. Minerals, 10(12): 1100. https://doi.org/10.3390/min10121100

Barbero E., Pandolfi L., Delavari M., Dolati A., Saccani E., Catanzariti R., Luciani V., Chiari M. and Marroni M., 2021a. The western Durkan Complex (Makran Accretionary Prism, SE Iran): A Late Cretaceous tectonically disrupted seamounts chain and its role in controlling deformation style. Geosci. Front., 12: 101106-1. https://doi.org/10.1016/j.gsf.2020.12.009

Barbero E., Zaccarini F., Delavari M., Dolati A., Saccani E., Marroni M. and Pandolfi L., 2021b. New evidence for Late Cretaceous plume-related seamounts in the Middle East sector of the Neo-Tethys: Constraints from geochemistry, petrology, and mineral chemistry of the magmatic rocks from the western Durkan Complex (Makran Accretionary Prism, SE Iran). Lithos, 396-397: 106228. https://doi.org/10.1016/j.lithos.2021.106228

Barbero E., Dilek Y., Festa A. and Saccani E., 2023a. Ophiolites and ophiolitic mélanges: Archives of Precambrian and Phanerozoic plate tectonics in orogenic belts. Geosys. Geoenv., 2 (3): 100191. https://doi.org/10.1016/j.geogeo.2023.100191

Barbero E., Di Rosa M., Pandolfi L., Delavari M., Dolati A., Zaccarini F., Saccani E., Marroni M., 2023b. Deformation history and processes during accretion of seamounts in subduction zones: The example of the Durkan Complex (Makran, SE Iran). Geosci. Front., 14 (2): 101522. https://doi.org/10.1016/j.gsf.2022.101522

Barbero E., Pandolfi L., Delavari M., Dolati A., Saccani E., Catanzariti R. and Marroni M., 2023c. The journey of the Band-e-Zeyarat ophiolite (Makran Accretionary Wedge, SE Iran) from the mid-ocean ridge to the accretionary complex: new insights from its sedimentary cover and associated basaltic dykes and sills. J. Geol. Soc., 180 (6): 2023-43. https://doi.org/10.1144/jgs2023-043

Barbero E., Pandolfi L., Delavari M., Dolati A., Saccani E., Di Rosa M. and Marroni M., 2025. A review of Mesozoic geodynamic evolution of the North Makran (SE Iran): A tale of a Neo-Tethyan ocean vanished due to two coexisting subduction zones. Gond. Res., 141: 74-101. https://doi.org/10.1016/j.gr.2025.01.009

Barrier E., Vrielynck B., Brouillet J.F. and Brunet M.F., 2018. Paleotectonic Reconstruction of the Central Tethyan Realm. Atlas of 20 maps. CCGM/CGMW, Paris.

Berberian F., Muir I.D., Pankhurst R.J. and Berberian M., 1982. Late Cretaceous and early Miocene andean-type plutonic activity in northern Makran and Central Iran. J. Geol. Soc. London, 139: 605-614. https://doi.org/10.1144/gsjgs.139.5.0605

Bonnet G., Agard P., Angiboust S., Monié P., Fournier M., Caron B. and Omrani J., 2020a. Structure and metamorphism of a subducted seamount (Zagros suture, Southern Iran). Geosphere, 16: 62-81. https://doi.org/10.1130/GES02131.1

Bonnet G., Agard P., Whitechurch H., Fournier M., Angiboust S., Caron B. and Omrani J., 2020b. Fossil seamount in southeast Zagros records intraoceanic arc to back-arc transition: New constraints for the evolution of the Neotethys. Gond. Res., 81: 423-444. https://doi.org/10.1016/j.gr.2019.12.008

Bröcker M., Omrani H., Berndt J. and Moslempour M.E., 2021. Unravelling metamorphic ages of suture zone rocks from the Sabzevar and Makran areas (Iran). J. Metam. Geol., 39: 1099-1129. https://doi.org/10.1111/jmg.12604

Burg J.-P., 2018. Geology of the onshore Makran accretionary wedge: Synthesis and tectonic interpretation. Earth Sci. Rev., 185: 1210-1231. https://doi.org/10.1016/j.earscirev.2018.09.011

Burg J.-P., Dolati A., Bernoulli D. and Smit J., 2013. Structural style of the Makran tertiary accretionary complex in SE Iran. In: Al Hosani K. et al. (Eds.). Lithosphere Dynamics and Sedimentary Basins. Springer, Heidelberg: 239-259. https://doi.org/10.1007/978-3-642-30609-9_12

Castillo P.R., 2006. An overview of adakite petrogenesis. Chin. Sci. Bull., 51(3): 257-268. https://doi.org/10.1007/s11434-006-0257-7

Chauvet F., Lapierre H., Maury R.C., Bosch D., Basile C., Cotten J., Brunet P. and Campillo S., 2011. Triassic alkaline magmatism of the Hawasina Nappes: Post-breakup melting of the Oman lithospheric mantle modified by the Permian Neotethyan Plume. Lithos, 122: 122-136. https://doi.org/10.1016/j.lithos.2010.12.004

Delavari M., Dolati A., Marroni M., Pandolfi L. and Saccani E., 2016. Association of MORB and SSZ ophiolites along the shear zone between Coloured Mélange and Bajgan Complexes (North Makran, Iran): Evidence from the Sorkhband area. Ofioliti, 41: 21-34. https://doi.org/10.4454/ofioliti.v41i1.432

Delavari M., Mehrabi B., Zelenski M., Chaplygin I., Nekrylov N., Shakeri A. and Taran Y., 2022. The Bazman and Taftan volcanoes of southern Iran: Implications for along-arc geochemical variation and magma storage conditions above the Makran low-angle subduction zone. J. Asian Earth Sci., 233: 105259. https://doi.org/10.1016/j.jseaes.2022.105259

Dercourt J., Zonenshian L.P., Ricou L.-E. et al., 1986. Geological evolution of the Tethys Belt from the Atlantic to the Pamirs since the Lias. Tectonophysics, 123: 241-315. https://doi.org/10.1016/0040-1951(86)90199-X

Dilek Y., 2003. Ophiolite concept and its evolution. In: Dilek Y. and Newcomb S. (Eds.). Ophiolite Concept and the Evolution of Geological Thought, Geol. Soc. Am. Spec. Pap. 373: 1-16. https://doi.org/10.1130/0-8137-2373-6.1

Dilek Y. and Furnes H., 2011. Ophiolite genesis and global tectonics: geochemical and tectonic fingerprinting of ancient oceanic lithosphere. Geol. Soc. Am. Bull., 123: 387-411. https://doi.org/10.1130/B30446.1

Dilek Y. and Furnes H., 2014. Ophiolites and Their Origins. Elements, 10 (2): 93-100. https://doi.org/10.2113/gselements.10.2.93

Dolati A., 2010. Stratigraphy, Structure Geology and Low-temperature Thermochronology Across the Makran Accretionary Wedge in Iran. PhD thesis, ETH Zurich.

Dolati A. and Burg J.-P., 2013. Preliminary fault analysis and paleostress evolution in the Makran Fold-and-Thrust Belt in Iran. In: Al Hosani K. et al. (Eds.). Lithosphere Dynamics and Sedimentary Basins. Springer, Heidelberg: 261-277. https://doi.org/10.1007/978-3-642-30609-9_13

Dorani M., Arvin M., Oberhänsli R. and Dargahi S., 2017. P-T evolution of metapelites from the Bajgan complex in the Makran accretionary prism, south eastern Iran. Geochemistry, 77: 459-475. https://doi.org/10.1016/j.chemer.2017.07.007

Esmaeili R., Xiao W., Ebrahimi M., Zhang J.E., Zhang Z., El-Rahman Y.A., Han C., Wan B., Ao S., Song D., Shahabi S. and Aouizerat A., 2019. Makran ophiolitic basalts (SE Iran) record late Cretaceous Neotethys plume-ridge interaction. Int. Geol. Rev., 62 (13-14): 1677-1697. https://doi.org/10.1080/00206814.2019.1658232

Esmaeili R., Xiao W., Griffin W.L., Moghadam H.S., Zhang Z., Ebrahimi M., Zhang J., Wan B., Ao S. and Bhandari S., 2020. Reconstructing the source and growth of the Makran Accretionary Complex: constraints from detrital zircon U/Pb geochronology. Tectonics, 39 (2): e2019TC005963. https://doi.org/10.1029/2019TC005963

Esmaeili R., Ao S., Moghadam H.S., Zhang Z., Griffin W.L., Ebrahimi M., Xiao W., Wan B. and Bhandari S., 2021. Amphibolites from Makran accretionary complex record Permian-Triassic Neo-Tethyan evolution. Int. Geol. Rev., 64 (11): 1594-1610. https://doi.org/10.1080/00206814.2021.1895036

Fitton J.G., Saunders A.D., Norry M.J., Hardarson B.S. and Taylor R.N., 1997. Thermal and chemical structure of the Iceland plume. Earth Planet. Sci. Lett., 153: 197-208. https://doi.org/10.1016/S0012-821X(97)00170-2

Fitton J.G., Saunders A.D., Kempton P.D. and Hardarson B.S., 2003. Does depleted mantle form an intrinsic part of the Iceland plume? Geochem. Geophys. Geosyst., 4(3): 1032. https://doi.org/10.1029/2002GC000424

Furnes H., Dilek Y., Zhao G., Safonova I. and Santosh M., 2020. Geochemical characterization of ophiolites in the Alpine-Himalayan Orogenic Belt. Earth Sci. Rev., 208: 103258. https://doi.org/10.1016/j.earscirev.2020.103258

Gaina C., van Hinsbergen D.J.J. and Spakman W., 2015. Tectonic interactions between India and Arabia since the Jurassic reconstructed from marine geophysics, ophiolite geology, and seismic tomography. Tectonics, 34: 875-906. https://doi.org/10.1002/2014TC003768

Ghasemi A. and Talbot C.J., 2006. A new tectonic scenario for the Sanandaj-Sirjan Zone (Iran). J. Asian Earth Sci., 26 (6): 683-693. https://doi.org/10.1016/j.jseaes.2005.01.003

Ghasemi Siani M., Mehrabi M., Neubauer F., Cao S. and Lentz D.R., 2021. Geochronology, geochemistry, and origin of plagiogranitic rocks and related granitic dikes in the Dar Gaz district, Kahnouj ophiolite complex, SE Iran: analysis of their petrogenesis in a back-arc tectonic setting. Lithos, 380-381. https://doi.org/10.1016/j.lithos.2020.105832

Ghasemi Siani M., Mehrabi B., Neubauer F. and Cao S., 2022a. Trace element geochemistry of zircons from the Kahnouj ophiolite complex: implications for petrogenesis and geodynamic setting. Arab. J. Geosci., 14: 1377. https://doi.org/10.1007/s12517-021-07575-5

Ghasemi Siani M., Mehrabi B., Ganerod M., Holwell D.A., Yang H.J. and Karimi Shahraki B., 2022b. Origin of Fe-Ti mineralization in the Late Jurassic to Early Cretaceous Kahnouj ophiolitic complex, Makran accretionary prism, SE Iran. Lithos, 426-427: 106784. https://doi.org/10.1016/j.lithos.2022.106784

Ghasemi Siani M., Mehrabi B., Yang H.J., Neubauer F., Huang K-F. and Liu Y-H., 2025. Whole-rock geochemistry and Sr-Nd-Pb isotope characteristics of gabbros from Kahnouj ophiolitic complex (SE Iran) in the Makran zone: Petrogenesis and tectonic implication. J. Afr. Earth Sci., 229: 105704. https://doi.org/10.1016/j.jafrearsci.2025.105704

Ghazi A.M., Hassanipak A.A., Mahoney J.J. and Duncan R.A., 2004. Geochemical characteristics, 40Ar-39Ar ages and original tectonic setting of the Band-e-Zeyarat/Dar Anar ophiolite, Makran accretionary Prism, S.E. Iran. Tectonophysics, 393: 175-196. https://doi.org/10.1016/j.tecto.2004.07.035

GholamiZadeh P., Wan B., Meinhold G., Esmaeili R. and Ebrahimi M., 2025a. Provenance evolution from subduction to arc-continent collision: An example from Zagros-Makran Transition Zone. Geosci. Front., 16 (4): 102079. https://doi.org/10.1016/j.gsf.2025.102079

GholamiZadeh P., Wan B., Garzanti E., Hu X., Esmaeili R. and Ebrahimi M., 2025b. Collision Timing and Provenance Shifts from the Late Oligocene to Middle Miocene in the Southeasternmost Zagros Orogen. Sci. Rep., 15: 6023. https://doi.org/10.1038/s41598-025-90186-x

Glennie K.W., Hughes Clarke M.W., Boeuf M.G.A., Pilaar W.F.H. and Reinhardt B.M., 1990. Inter-relationship of Makran-Oman Mountains belts of convergence. In: Robertson A.H.F., Searle M.P. and Ries A.C. (Eds.). The Geology and Tectonics of the Oman Region. Geol. Soc. London, Spec. Publ. 49 (1): 773-786. https://doi.org/10.1144/GSL.SP.1992.049.01.47.

Grando G. and McClay K., 2007. Morphotectonics domains and structural styles in the Makran accretionary prism, offshore Iran. Sedim. Geol., 196: 157-179. https://doi.org/10.1016/j.sedgeo.2006.08.009

Hajimohammadi F., Arvin M., Dargahi S., Khalatbari Jafari M. and Pan Y., 2025. Volcanic stratigraphy and vesicle analysis of pillow lavas in the North Makran complexes, southeastern Iran: Implications for emplacement depth of extrusive sequences. J. Asian Earth Sci., 291: 106649. https://doi.org/10.1016/j.jseaes.2025.106649

Hassanipak A.A., Ghazi A.M. and Wampler J.M., 1996. Rare earth element characteristics and K-Ar ages of the Bande-Zeyarat ophiolite complex, southeastern Iran. Can. J. Earth Sci., 33: 1534-1542. https://doi.org/10.1139/e96-116

Hunziker D., 2014. Magmatic and metamorphic history of the North Makran ophiolites and blueschists (SE Iran): Influence of Fe3+/Fe2+ ratios in blueschist facies minerals on geothermobarometric calculations. PhD thesis, ETH Zurich, 21778.

Hunziker D., Burg J.-P., Bouilhol P. and von Quadt A., 2015. Jurassic rifting at the Eurasian Tethys margin: Geochemical and geochronological constraints from granitoids of North Makran, southeastern Iran. Tectonics, 34: 571-593. https://doi.org/10.1002/2014TC003768

Hunziker D., Burg J.-P., Moulas E., Reusser E. and Omrani J., 2017. Formation and preservation of fresh lawsonite: geothermobarometry of the North Makran Blueschists, southeast Iran. J. Metamorph. Geol., 35 (8): 871-895. https://doi.org/10.1111/jmg.12258

Jagoutz O., Royden L., Holt A.F. and Becker T.W., 2015. Anomalously fast convergence of India and Eurasia caused by double subduction. Nat. Geosci., 8(6): 475-478. https://doi.org/10.1038/ngeo2418

Kakar M.I., Kerr A.C., Mahmmod K., Collins A.S., Khan M. and McDonald I., 2014. Supra-subduction zone tectonic setting of the Muslim Bagh Ophiolite, northwestern Pakistan: Insights from geochemistry and petrology. Lithos, 202-203: 190-206. https://doi.org/10.1016/j.lithos.2014.01.007

Kananian A., Juteau T., Bellon H., Darvishzadeh A., Sabzehi M., Whitechurch H. and Ricou L.-E., 2001. The ophiolite massif of Kahnuj (western Makran, southern Iran): new geological and geochronological data. C. R. Acad. Sci. Ser. IIA Earth Planet. Sci., 332: 543-552. https://doi.org/10.1016/S1251-8050(01)01573-8

Kopp C., Fruehn J., Flueh E.R., Reichert C., Kukowski N., Bialas J. and Klaeschen D., 2000. Structure of the Makran subduction zone from wide-angle and reflection seismic data. Tectonophysics, 329 (1-4): 171-191. https://doi.org/10.1016/S0040-1951(00)00195-5

Le Roex A.P., Dick H.J.B., Erlank A.J., Reid A.M., Frey F.A. and Hart S.R., 1983. Geochemistry, mineralogy and petrogenesis of lavas erupted along the southwest Indian ridge between the Bouvet triple junction and 11 degrees East. J. Petrol., 24 (3): 267-318. https://doi.org/10.1093/petrology/24.3.267

Marroni M. and Pandolfi L., 2007. The architecture of the Jurassic Ligure-Piemontese oceanic basin: tentative reconstruction along the northern Apennine-Alpine Corsica transect. Int. J. Earth Sci., 96: 1059-1078. https://doi.org/10.1007/s00531-006-0163-x

McCall G.J.H., 2002. A summary of the geology of the Iranian Makran. In: Clift P.D. et al. (Eds.). The Tectonic and Climatic Evolution of the Arabian Sea Region. Geol. Soc. London, Spec. Publ., 195: 147-204. https://doi.org/10.1144/GSL.SP.2002.195.01.10

McCall G.J.H. and Kidd R.G.W., 1982. The Makran southeastern Iran: the anatomy of a convergent margin active from Cretaceous to present. In: Leggett J.K. (Ed.). Trench-forearc geology. Geol. Soc. London, Spec. Publ., 10: 387-397. https://doi.org/10.1144/GSL.SP.1982.010.01.26

McCall G.J.H., 1983. Mélanges of the Makran, southeastern Iran. In: McCall G.J.H. (Ed.). Ophiolitic and related mélanges, Benchmark Papers in Geology 66. Hutchinson Ross, Stroudsburg: 292-299. *(no DOI — volume editoriale)*

McCall G.J.H., 1985. Explanatory text of the Minab Quadrangle Map; 1:250,000; No. J13. Geol. Surv. Iran, Tehran, pp. 530.

McCall G.J.H., 1997. The geotectonic history of the Makran and adjacent areas of southern Iran. J. Asian Earth Sci., 15: 517-531. https://doi.org/10.1016/S0743-9547(97)00005-9

Metcalfe I., 2013. Gondwana dispersion and Asian accretion: Tectonic and palaeogeographic evolution of eastern Tethys. J. Asian Earth Sci., 66: 1-33. https://doi.org/10.1016/j.jseaes.2012.12.020

Moghadam H.S., Mosaddegh H. and Santosh M., 2013. Geochemistry and petrogenesis of the Late Cretaceous Haji-Abad ophiolite (Outer Zagros Ophiolite Belt, Iran): implications for geodynamics of the Bitlis-Zagros suture zone. Geol. J., 48: 579-602. https://doi.org/10.1002/gj.2467

Moghadam H.S. and Stern R.J., 2015. Ophiolites of Iran: Keys to understanding the tectonic evolution of SW Asia: (II) Mesozoic ophiolites. J. Asian Earth Sci., 100: 31-59. https://doi.org/10.1016/j.jseaes.2014.12.016

Moghadam H.S., Bröcker M., Griffin W.L., Li X.H., Chen R.X. and O'Reilly S.Y., 2017. Subduction, high-P metamorphism, and collision fingerprints in South Iran: Constraints from zircon U-Pb and mica Rb-Sr geochronology. Geochem. Geophys. Geosyst., 18: 306-332. https://doi.org/10.1002/2016GC006585

Moghadam H.S., Li Q., Griffin W., Chiaradia M., Hoernle K., O'Reilly S. and Esmaeili R., 2021. The Middle-Late Cretaceous Zagros ophiolites, Iran: Linking of a 3000 km swath of subduction initiation fore-arc lithosphere from Troodos, Cyprus to Oman. Geol. Soc. Am. Bull., 134 (5-6): 1414-1442. https://doi.org/10.1130/B35737.1

Moghadam H.S., Arai S., Griffin W.L., Khedr M., Saccani E., Henry H., O'Reilly S.Y. and Ghorbani G., 2022. Geochemical variability among stratiform chromitites and ultramafic rocks from Western Makran, South Iran. Lithos, 412-413: 106591. https://doi.org/10.1016/j.lithos.2021.106591

Mohammadi A., Burg J.-P., Winkler W., Ruh J. and von Quadt A., 2016. Detrital zircon and provenance analysis of Late Cretaceous-Miocene onshore Iranian Makran strata: Implications for the tectonic setting. Geol. Soc. Am. Bull., 128 (9-10), 1481-1499. https://doi.org/10.1130/B31361.1

Mohammadi A., Burg J.-P., Guillong M. and Von Quadt A., 2017. Arc magmatism witnessed by detrital zircon U-Pb geochronology, Hf isotopes and provenance analysis of Late Cretaceous-Miocene sandstones of onshore Western Makran. Am. J. Sci., 317 (8): 941-964. https://doi.org/10.2475/08.2017.03

Monsef I., Monsef R., Mata J., Zhang Z., Pirouz M., Rezaeian M., Esmaeili R. and Xiao W., 2018. Evidence for an early-MORB to fore-arc evolution within the Zagros suture zone: Constraints from zircon U-Pb geochronology and geochemistry of the Neyriz ophiolite (South Iran). Gond. Res., 62: 287-305. https://doi.org/10.1016/j.gr.2018.03.002.

Moslempour M.E., Khalatbari-Jafari M., Ghaderi M., Yousefi H. and Shahdadi S., 2015. Petrology, geochemistry, and tectonics of the extrusive sequence of Fannuj-Maskutan Ophiolite, southeastern Iran. J. Geol. Soc. India, 85: 604-618. https://doi.org/10.1007/s12594-015-0255-y

Muñoz-Montecinos J., Angiboust S. and Garcia-Casco A., 2021. Blueschist-facies paleo-earthquakes in a serpentinite channel (Zagros suture, Iran) enlighten seismogenesis in Mariana-type subduction margins. Earth Planet. Sci. Lett., 573: 117135. https://doi.org/10.1016/j.epsl.2021.117135

Omrani H., Moazzen M., Oberhänsli R. and Moslempour M.E., 2017. Iranshahr blueschist: subduction of the inner Makran oceanic crust. J. Metam. Geol., 35: 373-392. https://doi.org/10.1111/jmg.12236.

Pandolfi L., Barbero E., Marroni M., Delavari M., Dolati A., Di Rosa M., Frassi C., Langone A., Farina F., MacDonald C.S. and Saccani E., 2021. The Bajgan Complex revealed as a Cretaceous ophiolite-bearing subduction complex: A key to unravel the geodynamics of Makran (southeast Iran). J. Asian Earth Sci., 222: 104965. https://doi.org/10.1016/j.jseas.2021.104965

Parlak O., Dunk I., Karaoğlan F., Kusky T.M., Zhang C., Wang L., Koepke J., Billor Z., Hames W.E., Şimşek E., Şimşek G., Şimşek T. and Öztürk S.E., 2019. Rapid cooling history of a Neotethyan ophiolite: evidence for contemporaneous subduction initiation and metamorphic sole formation. Geol. Soc. Am. Bull., 131 (11-12): 2011-2038. https://doi.org/10.1130/B35040.1

Pearce J.A., 1983. Role of the Sub-continental Lithosphere in magma Genesis at Active Continental Margin. In: Hawkesworth C.J. and Norry M.J. (Eds.). Continental Basalts and Mantle Xenoliths. Nantwich, Shiva Publ. Co.; 230-249.

Pearce J.A., 1996. A user's guide to basalt discrimination diagrams. In: Wyman D.A. (Ed.), Trace Element Geochemistry of Volcanic Rocks: Applications for Massive Sulphide Exploration. Min. Ass. of Canada, Short Course Notes, 12: 79-113.

Pearce J.A., 2008. Geochemical fingerprinting of oceanic basalts with applications to ophiolite classification and the search for Archean oceanic crust. Lithos, 100: 14-48. https://doi.org/10.1016/j.lithos.2007.06.016

Pirnia T., Saccani E., Torabi G., Chiari M., Gorican S. and Barbero, E., 2019. Cretaceous tectonic evolution of the Neo-Tethys in Central Iran: Evidence from petrology and age of the Nain-Ashin ophiolitic basalts. Geosci. Front., 11 (1): 57-81. https://doi.org/10.1016/j.lithos.2007.06.016

Platt J.P., Leggett J.K., Young J., Raza H. and Alam S., 1985. Large-scale sediment underplating in the Makran accretionary prism, southwest Pakistan. Geology, 13 (7): 507-511. https://doi.org/10.1130/0091-7613(1985)13%3C507:LSUITM%3E2.0.CO;2

Rajabzadeh M.A. and Moosavinasab Z., 2013. Mineralogy and distribution of Platinum-Group Minerals (PGM) and other solid inclusions in the Faryab ophiolitic chromitites, Southern Iran. Mineral. Petrol.,107: 943-962. https://doi.org/10.1007/s00710-012-0265-z

Regard V., Hatzfeld D., Molinaro M., Aubourg C., Bayer R., Bellier O., Yamini-Fard F., Peyret M. and Abbassi M., 2010. The transition between Makran subduction and the Zagros collision: recent advances in its structure and active deformation. Geol. Soc. London, Spec. Publ. 330 (1); 43-64. https://doi.org/10.1144/SP330.4

Richards J.P. and Kerrich R., 2007. Adakite-Like Rocks: Their Diverse Origins and questionable role in metallogenesis. Econ. Geol., 102: 537-576. https://doi.org/10.2113/gsecongeo.102.4.537

Ricou L.E., 1994. Tethys reconstructed: plates continental fragments and their boundaries since 260Ma from Central America to South-eastern Asia. Geodinam. Acta, 7: 169-218. https://doi.org/10.1080/09853111.1994.11105266

Robertson A.H.F. and Searle M.P., 1990. The northern Oman Tethyan continental margin: stratigraphy, structure, concepts and controversies. In: A.H.F. Robertson, Searle M.P. and Ries A.C. (Eds.). The Geology and Tectonics of the Oman Region, Geol. Soc. London, Spec. Publ., 49; 3-25. https://doi.org/10.1144/GSL.SP.1992.049.01.02

Rolland Y., Hässig M., Bosch D., Bruguier O., Melis R., Galoyan G., Topuz G., Sahakyan L., Avagyan A. and Sosson M., 2020. The East Anatolia-Lesser Caucasus ophiolite: An exceptional case of large-scale obduction, synthesis of data and numerical modelling. Geosci. Front., 11 (1): 83-108. https://doi.org/10.1016/j.gsf.2018.12.009

Saccani E., 2015. A new method of discriminating different types of post-Archean ophiolitic basalts and their tectonic significance using Th-Nb and Ce-Dy-Yb systematics. Geosci. Front., 6: 481-501. https://doi.org/10.1016/j.gsf.2014.03.006

Saccani E., Delavari M., Beccaluva L. and Amini S.A., 2010. Petrological and geochemical constraints on the origin of the Nehbandan ophiolitic complex (eastern Iran): Implication for the evolution of the Sistan Ocean. Lithos, 117: 209-228. https://doi.org/10.1016/j.lithos.2010.02.016

Saccani E., Allahyari K., Beccaluva L. and Bianchini G., 2013. Geochemistry and petrology of the Kermanshah ophiolites (Iran): Implication for the interaction between passive rifting, oceanic accretion, and plume-components in the Southern Neo-Tethys Ocean. Gond. Res., 24: 392-411. https://doi.org/10.1016/j.gr.2012.10.009

Saccani E., Dilek Y. and Photiades A., 2017. Time-progressive mantle-melt evolution and magma production in a Tethyan marginal sea: A case study of the Albanide-Hellenide ophiolites. Lithosphere, 10: 35-53. https://doi.org/10.1130/L602.1

Saccani E., Delavari M., Dolati A., Marroni M., Pandolfi L., Chiari M. and Barbero E., 2018. New insights into the geodynamics of Neo-Tethys in the Makran area: Evidence from age and petrology of ophiolites from the Coloured Mélange Complex (SE Iran). Gond. Res., 62: 306-327. https://doi.org/10.1016/j.gr.2017.07.013

Saccani E., Delavari M., Dolati A., Pandolfi L., Barbero E., Brombin V. and Marroni M., 2022a. Geochemistry of volcanic rocks and dykes from the Remeshk-Mokhtarabad and Fannuj-Maskutan Ophiolites (Makran Accretionary Prism, SE Iran): New constraints for magma generation in the Middle East Neo-Tethys. Geosys. Geoenv., 3: 100140. https://doi.org/10.1016/j.geogeo.2022.100140

Saccani E., Delavari M., Dolati A., Pandolfi L., Barbero E., Tassinari R. and Marroni M., 2022b. Geochemistry of basaltic blueschists from the Deyader Metamorphic Complex (Makran Accretionary Prism, SE Iran): New constraints for magma generation in the Makran sector of the Neo-Tethys. J. Asian Earth Sci.: 105141. https://doi.org/10.1016/j.jseaes.2022.105141

Saccani E., Barbero E., Delavari M., Dolati A., Brombin V., Marroni M. and Pandolfi L., 2024. Geochemistry and magmatic petrology of metaophiolites from the Bajgan Complex (Makran Accretionary Prism, SE Iran): New insights on the nature of the Early Cretaceous Middle East Neo-Tethys. J. Geol. Soc., 181: 2024-043. https://doi.org/10.1144/jgs2024-043

Safonova I., Maruyama S., Kojima S., Komiya T., Krivonogov S. and Koshida K., 2016. Recognizing OIB and MORB in accretionary complexes: a new approach based on ocean plate stratigraphy, petrology, and geochemistry. Gond. Res., 33: 92-114. https://doi.org/10.1016/j.gr.2015.06.013

Şengör A.M.C., Altiner D., Cin A., Ustaömer T. and Hsü K.J., 1988. Origin and assembly of the Tethyside orogenic collage at the expense of Gondwana Land. In: Audley-Charles M.G. and Hallam A. (Eds.). Gondwana and Tethys, Geol. Soc. London, Spec. Publ. 37(1); 119-181. https://doi.org/10.1144/GSL.SP.1988.037.01.09

Sepidbar F., Lucci F., Biabangard H., Zaki Khedr M. and Jiantang P., 2020. Geochemistry and tectonic significance of the Fannuj-Maskutan SSZ-type ophiolite (Inner Makran, SE Iran). Int. Geol. Rev., 62(16): 2077-2104. https://doi.org/10.1080/00206814.2020.1753118.

Shaker Ardakani A.R., Arvin M., Oberhänsli R., Mocek B. and Moeinzadeh S.H., 2009. Morphology and petrogenesis of pillow lavas from the Ganj Ophiolitic Complex, Southeastern Kerman. Iran. J. Sci. Islam. Rep. Iran, 20: 139-151.

Shervais J.W.,1982. Ti-V plots and the petrogenesis of modern ophiolitic lavas. Earth Planet. Sci. Lett., 59: 101-118. https://doi.org/10.1016/0012-821X(82)90120-0

Shervais J.W., 2001. Birth, death, and resurrection: The life cycle of suprasubduction zone ophiolites. Geochem. Geophys. Geosyst., 2: 200GC000080. https://doi.org/10.1029/2000GC000080

Stampfli G.M., 2000. Tethyan oceans. In: Bozkurt E., Winchester J. and Piper J.A. (Eds.). Tectonics and Magmatism in Turkey and the Surrounding Area, Geol. Soc. London, Spec. Publ. 173; 1-23. https://doi.org/10.1144/GSL.SP.2000.173.01.01

Stampfli G.M., and Borel G.D., 2002. Western Alps geological constraints on western Tethyan reconstruction. In: Rosenbaum G. and Lister G.S. (Eds.). Reconstruction of the evolution of the Alpine-Himalayan orogen, J. Virt. Expl. 8; 77-106. https://doi.org/10.1144/GSL.SP.2000.173

Stöcklin J., 1968. Structural history and tectonics of Iran: A review. Bull. Am. Ass. Petrol. Geol., 52: 1229-1258. https://doi.org/10.1306/5D25C4A5-16C1-11D7-8645000102C1865D

Sun S.-S. and McDonough W.F., 1989. Chemical and isotopic systematics of oceanic basalts: implications for mantle composition and processes. In: Saunders A.D. and Norry M.J. (Eds.). Magmatism in oceanic basin, Geol. Soc. London, Spec. Publ. 42(1); 313-345. https://doi.org/10.1144/GSL.SP.1989.042.01.19

Torsvik T.H., van der Voo R., Preeden U., Mac Niocaill C., Steinberger B., Doubrovine P.V., van Hinsbergen D.J.J., Domeier M., Gaina C., Tohver E., Meert J., McCausland P. and Cocks L.R.M., 2012. Phanerozoic polar wander, palaeogeography and dynamics. Earth-Sci. Rev., 114(3-4): 325-368. https://doi.org/10.1016/j.earscirev.2012.06.007

Received, February 17, 2026
Accepted, May 8, 2026